Ocean crust accretion along a high-temperature detachment fault in the Oman ophiolite: A structural and petrological study of the Bahla massif

Bénédicte Abily, Georges Ceuleneer, Mathieu Rospabé, Mary-Alix Kaczmarek, Marie Python, Michel Grégoire, Benoit Benoit, Matthew Rioux

Ocean crust accretion along a high-temperature detachment fault in the Oman ophiolite: a structural and petrological study of the Bahla massif.

Bénédicte Abily[1], Georges Ceuleneer[1(*)], Mathieu Rospabé[2], Mary-Alix Kaczmarek[1], Marie Python[3], Michel Grégoire[1], Mathieu Benoit[1] and Matthew Rioux[4]

[1] Géosciences Environnement Toulouse, OMP, CNRS–UMR 5563, 14 av. E. Belin, 31400 Toulouse, France.

[2] Research Institute for Marine Geodynamics (IMG), Japan Agency for Marine-Earth Science and Technology (JAMSTEC), 2-15 Natsushima, Yokosuka, Kanagawa 237-0061, Japan.

[3] Hokkaido University, Department of Natural History Science, Division of Earth and Planetary Systems Sciences, 060-0810, North 10, West 8, Kita-ku, Sapporo, Japan.

[4] University of California, Department of Earth Science, 1006 Webb Hall, Santa Barbara, CA 93106, USA.

(*) Corresponding author

Abstract

The Bahla massif exposes the lower crustal section of the Oman ophiolite located close to the thrust front of the Semail nappe. It is affected by intense faulting previously attributed to tectonic events that dismembered a classical ophiolitic sequence during or after the obduction. Here we show that most of this complexity is primary, inherited from syn-accretion tectonics. The crustal section is exposed in a 15 by 8 km tectonic enclave surrounded by mantle peridotite. Its northern boundary corresponds to a major, steeply dipping normal fault striking WNW-ESE, at low angle to the paleo-ridge axis. Movement along this fault was accommodated by intense plastic deformation of the crustal cumulates and adjacent mantle peridotites at temperature conditions ≥ 900°C. The thickness of the deformed zone reaches several hundred meters. The flattening of the cumulate layering away from the fault is correlated to a decrease in the deformation intensity. Undeformed olivine-gabbro dykes cross-cut this "tectonic Moho" indicating that the tilting occurred before the end of the igneous activity. To the southwest, the crustal enclave is bounded by a NW-SE trending transtentional shear zone that was active in the amphibolite to greenschist facies and was intensely injected by syn- to post-kinematic gabbronorite and tonalite/trondhjemite dykes and plugs. The age of one felsic sample (95.214 ± 0.032 Ma, high-precision U-Pb zircon dating) is within error of the age of intrusive felsic intrusions into the mantle and lowermost axial crust from the length of the Oman ophiolite, which slightly post-dates the mean crystallization age of the Semail crust (V1 magmatism;

96.1–95.6 Ma). Other contacts are low temperature features including cataclastic faults, serpentine-carbonate breccias and flat-lying décollements.

Parent melts of the Bahla crustal cumulates were more siliceous and hydrous, i.e. more andesitic, than typical mid-ocean ridge basalt (MORB) as deduced from the frequent occurrence of early crystallizing orthopyroxene (opx) and late crystallizing amphibole. Some facies such as cumulate harzburgite and opx-troctolite have not been documented elsewhere in the Oman ophiolite and may be specific to the tectonic context in which the frontal massifs accreted. The chemical composition of the lower crustal cumulates can be accounted for by the hybridization in various proportions between MORB and a primitive andesite from a depleted source whose origin can be looked for in melts from a nascent subduction zone or from high temperature hydrothermal processes.

The structure of the Bahla lower crustal section is reminiscent of the plutonic growth faults documented along present-day slow-spreading centres in both mid-ocean ridge and back arc settings. The distinctive characteristics of the Moho and lower crustal section in the Bahla massif are tentatively related to their position at the leading edge of the ophiolite, i.e. closer to the Arabian continental margin at the time of accretion than the massifs from the internal part of the ophiolite that have a more continuous and less deformed lower crust. It indicates that the style of crustal accretion may have changed during the opening of the oceanic basin from which the Oman ophiolite issued.

Keywords: Oman; ophiolite; oceanic crust; detachment faults; plutonic growth faults.

1. Introduction

The Semail ophiolite (Oman and UAE) is an upper Cretaceous remnant of the vanished Tethys Ocean (Ricou, 1971; Glennie et al., 1973). It is widely considered as a fossil analog of oceanic spreading centres, although its tectonic setting (mid-ocean ridge *vs*. subduction related) is still debated. Our understanding of the structure and dynamics of axial magma chambers has been largely nurtured by observations in its plutonic section. Surprisingly, a glance to the literature reveals that the petrologic nature of this unit has been determined in a limited number of spots. A bias clearly exists in favor of exposures of continuous and un-faulted sections of layered cumulates. More specifically, the plutonic section remains largely unexplored where it is adjacent to the thrust front of the Semail nappe. The complex structures observed there were interpreted in geological maps as an imprint of thin-skin tectonics related to the obduction or

more recent events (Wyns et al., 1992; Béchennec et al., 1992). This situation looked unattractive to the petrologists interested by oceanic spreading centers processes. The present paper is devoted to the first combined structural, petrological and geochemical study of one of these frontal massifs, cropping out around the city of Bahla (Fig. 1a).

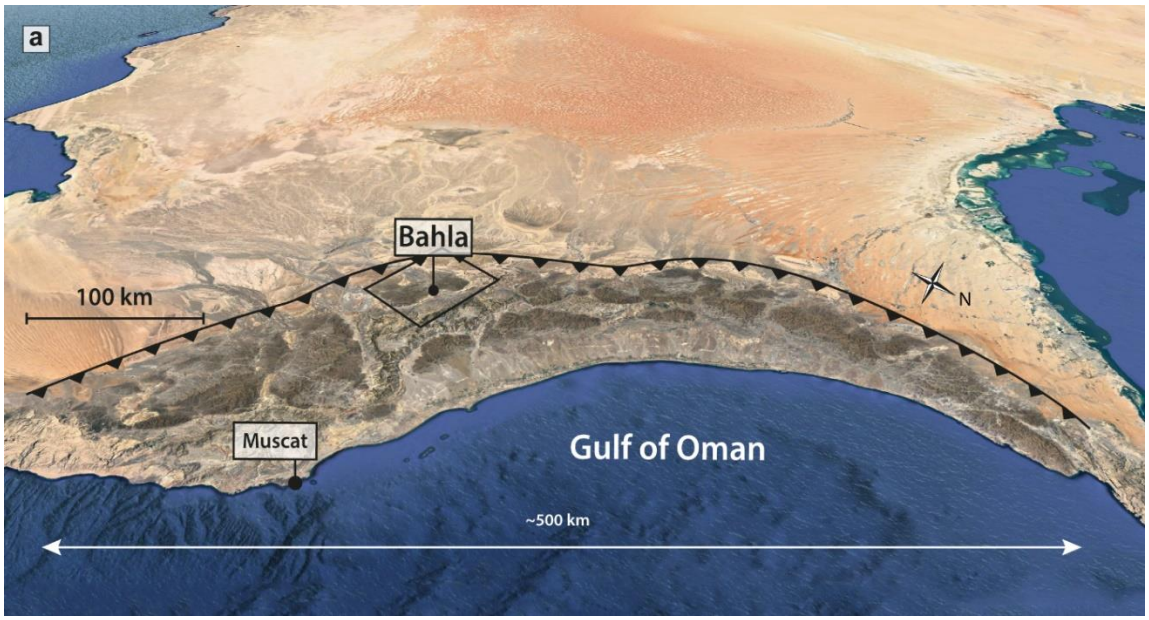

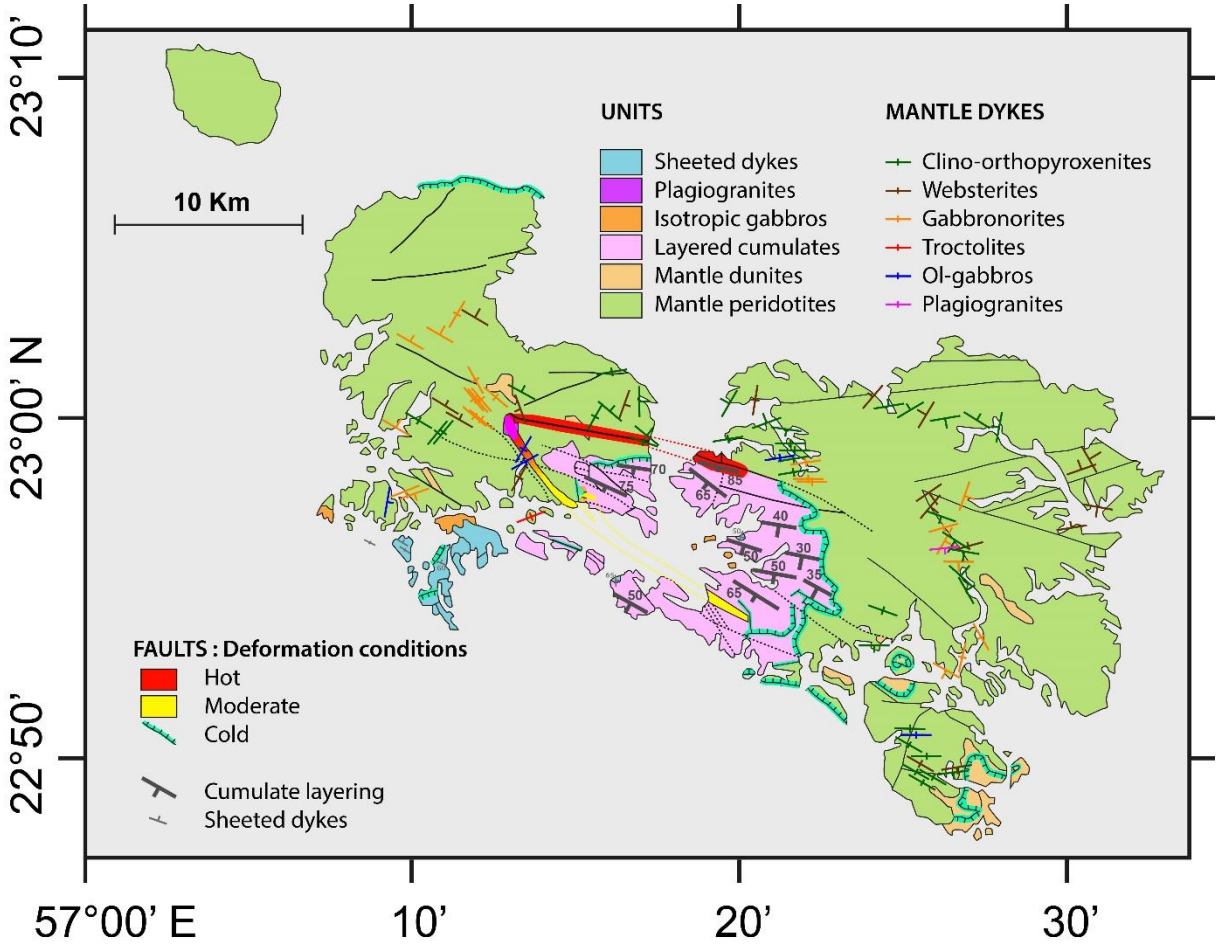

Fig. 1. (a) Location of the Bahla massif on a Google Earth image of the Northern Oman Mountains. The approximate position of the thrust front of the ophiolite is shown by the black line with triangles. The scale is indicative and valid only for the foreground of the image due to the oblique view. (b) Geological map of the Bahla massif modified after Wyns et al. (1992) and Béchennec et al. (1992). The orientation of the layering (averaged per site) is shown as grey symbols.

During the course of a systematic survey of the lower crustal cumulates of Oman, we observed, in the Bahla massif, very high temperature deformation structures along the mantle-crust boundary. Simple field and petrographic arguments allowed us to discard a late origin of these features which left the door open to two main avenues of interpretations: (1) the imprint of early intra-oceanic thrusting (that can be viewed as nascent subduction) in a near ridge environment (cf. Boudier et al., 1988); (2) the trace of syn-accretion faults reminiscent of those observed along present-day oceanic spreading centers (e.g. Blackman et al., 1998; Dick et al., 2008; Ildefonse et al., 2007; Escartin et al., 2008; Harigane et al., 2011; Sauter et al., 2021). Here we present structural evidence allowing us to decipher between these two hypotheses. We also show that high temperature deformation may interfere with the petrological evolution of the lower crustal cumulates of Oman and account for some of their puzzling characteristics.

2. Tectonic setting of the Oman ophiolite: an open question

The Oman ophiolite is one of the largest fragment of oceanic lithosphere exposed on land. It is particularly well preserved because it is not yet affected by continental collision between Arabia and Eurasia (e.g. Coleman, 1981). Igneous accretion of the ophiolite occurred in a narrow time lapse (96.1 to 95.6 Ma, Rioux et al., 2013, 2021a). This event was largely synchronous with the intra-oceanic thrusting of the future ophiolite. This is attested by the overlap between the accretion age and the age of the metamorphic sole (Rioux et al., 2016) and by structural and petrological evidence for the existence of segments of the spreading center itself preserved within the ophiolite (Ceuleneer, 1991; Ceuleneer et al., 1988, 1996; MacLeod and Rothery, 1992; Python and Ceuleneer, 2003). The thrusting of the oceanic lithosphere on the continental margin was completed during Maestrichtian times (~70 m.y. ago) (Glennie et al., 1973). Continental subduction preceded this event as witnessed by the high-pressure metamorphism that affected the northeastern tip of the Oman margin ~80 m.y. ago (Goffé et al., 1988; Warren et al., 2003; Gray et al., 2004, 2005; Searle et al., 2004; Yamato et al., 2007).

The tectonic setting (subduction-related basins vs. more open ocean ridge segments) during the igneous accretion of the Oman ophiolite is a long-standing debate (e.g. Coleman, 1981;

Pallister and Hopson, 1981; Hopson et al., 1981; Pearce et al., 1981; Searle et al., 2004; Gray et al., 2005; Ishikawa et al., 2005; Boudier and Nicolas, 2007; Warren et al., 2007, MacLeod et al., 2013; Belgrano and Diamond, 2019; De Graaf et al., 2019; Agard et al., 2020). Plate tectonic reconstructions, imprecise during the Cretaceous normal magnetic superchron, are of little help to solve this specific problem (Granot et al., 2012). The extrusive section of the ophiolite includes lavas with MORB and depleted andesitic affinities (Alabaster et al., 1982; Pearce et al., 1981). Ernewein et al. (1988) introduced the notion of V1 and V2 episodes to refer respectively to these two igneous series, assuming that MORB lavas are overlain by the depleted andesitic lava flows, although the correlation between the geochemical signature and the stratigraphic position of the lavas is not perfect (Einaudi et al., 2003; Belgrano and Diamond, 2019). A similar petrological dichotomy between a MORB and a depleted andesitic kindred was also found in the mantle dykes, former feeding channels of the crustal section (Benoit et al., 1999; Python and Ceuleneer, 2003; Python et al., 2008) and in the layered crustal cumulates themselves (Smewing, 1981; Juteau et al., 1988; Yamasaki et al., 2006; Adachi and Miyashita, 2003; Clénet et al., 2010). The existence, if any, of a relative chronology (i.e. "P1 *vs*. P2") for the emplacement and crystallization of the two plutonic series is difficult to determine at the global scale, authors working on different outcrops and different lithologies reaching contrasted conclusions (e.g. Benoit et al., 1999; Python and Ceuleneer, 2003; Haase et al., 2016; Goodenough et al., 2014; Rospabé et al., 2017; De Graaf et al., 2019).

The spreading rate at the time of the igneous accretion of the Oman ophiolite is another open question. This parameter is largely unconstrained. Even if the context was clearly the one of high melt supply to the crust, this does not necessarily imply a high spreading rate. Structural evidence like mantle flow pattern (Ceuleneer et al., 1988), the existence of a layered lower crustal section and of a well-developed sheeted dyke complex (Hopson et al., 1981; Pallister and Hopson, 1981; Pallister, 1981) are not definitive arguments. Recently published high precision ages on plagiogranites and evolved oxide gabbro from the Wadi Tayin massif tend to support fast (≥ 5 cm.y^{-1}) spreading rates during the accretion of this massif located in the internal and southeastern part of the ophiolite (Rioux et al., 2012).

The wealth of data obtained on the Oman ophiolite during the last decades reveals its heterogeneity and the complexity of its igneous history that may include assimilation of peridotite and/or formerly crystallized crust (e.g. Benoit et al., 1999; Koepke et al., 2009; Rioux et al., 2012; Abily and Ceuleneer, 2013; Rospabé et al., 2017, 2018), ridge propagation (e.g. Andronicos et al., 2008), syn-magmatic faults (Abily et al., 2011; Rospabé et al., 2019) and

off-axis magmatism (Jousselin and Nicolas, 2000; Rioux et al., 2013). Clearly, this diversity needs to be taken into account in the interpretation of the Oman ophiolite as a whole.

3. Methods

3.1. Electron microprobe

Major and minor element compositions of the main magmatic phases (olivine, clinopyroxene, orthopyroxene, plagioclase) were determined using the electron microprobe CAMECA SX50 at Toulouse University and CAMECA SX100 at Brest University. A standard analysis program with an accelerating voltage of 15 kV and a beam current of 10 to 20 nA was used. Counting time was 10 s on the peak and 5 s on the background. The detection limits were similar for both instruments with values of ~0.07% for Al_2O_3 and Na_2O and ~0.09% for TiO_2 and Cr_2O_3 for all phases analyzed.

3.2. LA-ICP-MS

Concentrations of trace elements in cpx were determined by LA-ICP-MS, at the Observatoire Midi-Pyrénées (Paul Sabatier University, Toulouse). This allowed in situ analysis of Cpx in 120 □m thick polished sections. The Agilent 7500 ce ICPMS apparatus was coupled to a Cetac LSX-200 laser ablation module with a 266 nm frequency-quadrupled Nd-YAG laser. The NIST 610 glass was used as the external standard while the NIST 612 glass was used as a reference material to control the quality of measurements. Each analysis was normalized using CaO values determined by electron microprobe. A beam diameter of 50-100 μm, a frequency of 10 Hz and a scanning rate of 20 mm/s were used. The theoretical detection limits were between 10 and 20 ppb for rare earth elements (REE), Ba, Th, U, Zr and 2 ppm for Ti. The relative precision and accuracy for a laser analysis ranges from 1 to 10%. The data reduction was carried out with the Glitter software (Griffin, 2008).

3.3. Electron Backscatter Diffraction (EBSD).

EBSD analyses have been performed on 5 samples where olivine, pyroxenes and plagioclase have been analyzed. Before analyses, a mechanic-chemical polishing using a Vibromet was applied for 1 h15 with a colloidal silica suspension (pH 10) to remove mechanically-induced surface damage. The EBSD camera HKL Advanced Nordlys Nano from Oxford Instruments is attached to a JEOL 7100 electronic microscope, located at the microcharacterization centre Raimond Castaing, University Paul Sabatier, Toulouse, France.

The microscope working conditions include an acceleration voltage of 20 kV, a probe current of 16 nA, with a stage tilt of 70°, a working distance of 16-17 mm and camera settings are 4x4 binning and low (0) gain. Automatic indexing was performed using AZTec software (version 3.5) from Oxford Instruments, with different step size (15, 20 or 25 µm) according to the grain size. Data were processed using Channel 5 package. Measurements with a mean angular deviation (MAD) greater than 1.3 were removed, and grains were then calculated by imposing an orientation difference smaller than 10° for any two neighboring measurements belong to the same grain. Grains with a surface smaller than 10 pixels were removed to avoid bias caused by potential indexing error. The maps were compared with band contrast maps to ensure that the treatment did not compromise the data. The multiple uniform density (mud) and the J-index, which is the measure of the fabric strength (Bunge, 1982) are reported on figure 8.

4. Results

4.1. Structure of the Bahla massif

4.1.1. General structure

The more complete information on the general structure of the Bahla massif are reported in the geological maps of the area (Wyns et al., 1992; Béchennec et al., 1992) and in the synthetic maps of the high temperature structural features of the Oman ophiolite (Nicolas et al., 2000). The Bahla massif is a 45 km long and 15 km wide ellipsoidal body elongated along a WNW-ESE direction parallel to the local strike of the paleo-spreading ridge axis (MacLeod and Rothery, 1992) (Fig. 1b). The mantle section represents the main part of the massif; it is made essentially of harzburgites presenting the typical imprint of high temperature plastic flow acquired at “asthenospheric” conditions (Ceuleneer et al., 1988; Nicolas et al., 1988), with locally abundant dunitic and pyroxenite bands. These rocks are cut by dykes filled mostly with pyroxenitic and gabbronoritic assemblages, with rare troctolites, gabbros, diorites and trondhjemites (Python and Ceuleneer, 2003).

The crustal section represents only one fifth of the massif area and crops out essentially in its central part. The lower crust adopts the shape of a 15 km long and 8 km wide ellipse whose long axis is parallel to the general elongation of the massif (Fig. 1b). To the North, West and East, it is surrounded by mantle peridotites. The upper crust, including the base of the sheeted

dyke complex, is exposed as small scattered outcrops emerging from quaternary deposits in the southern part of the massif. In geological maps some outcrops of this area are reported as mantle peridotites; they are mostly ultramafic cumulates (olivine cumulates with poikilitic pyroxenes) cut by diabase dykes generally striking N120°E and dipping 60° - 70° to the NE.

The map pattern summarized above is not an expression of topography alone. The crustal section of Bahla is actually a tectonic enclave in a mantle host and not the un-eroded remnant of a formerly continuous crustal layer overlying the mantle section, which is the most common situation in other massifs of the Oman ophiolite. This structural specificity of the Bahla massif is primarily attributable to tectonics. Here below is a description of the contrasting tectonic styles we observed along these faulted mantle-crust contacts.

4.1.2. The northern contact

Along the northern mantle-crust boundary, the igneous textures of the layered cumulates are intensely overprinted by plastic deformation. There, the mantle-crust boundary (we will call the "Moho" for the sake of simplicity) is actually part of a WNW-ESE-trending sub-vertical ductile shear zone (in red on Fig. 1b) penetrating to the West and to the East in the mantle section. Its lateral extent reaches 15 km, being interrupted by lower temperature faults described below (§4.1.3 and §4.1.4). It affects the mantle peridotites and the lower crustal cumulates on both sides of the Moho on a thickness exceeding 1 km.

The mantle peridotites have a porphyroclastic texture and are highly foliated (Fig. 2a). This intense deformation is underlined by transposed pyroxenite bands (Fig. 2b). On the crustal side, mafic cumulates are intensely deformed too; they display flaser and gneissic textures (Fig. 2c) with local development of a spectacular tectonic banding enhanced by centimetre-thick white bands of anorthosite (Fig. 2d).

The primary igneous mineral assemblage is generally not modified, although locally, we observe the development of hornblende rims around pyroxene porphyroclasts. The deformed cumulates have medium-grained equigranular granoblastic textures with sutured grain boundaries diagnostic of efficient diffusion enhancing grain boundary migration. Intra-crystalline features like undulose extinction, bending and mechanical twins are present but are not common, which is diagnostic of efficient recovery, and thus of high-temperature making possible sub-solidus diffusion.

Fig 2

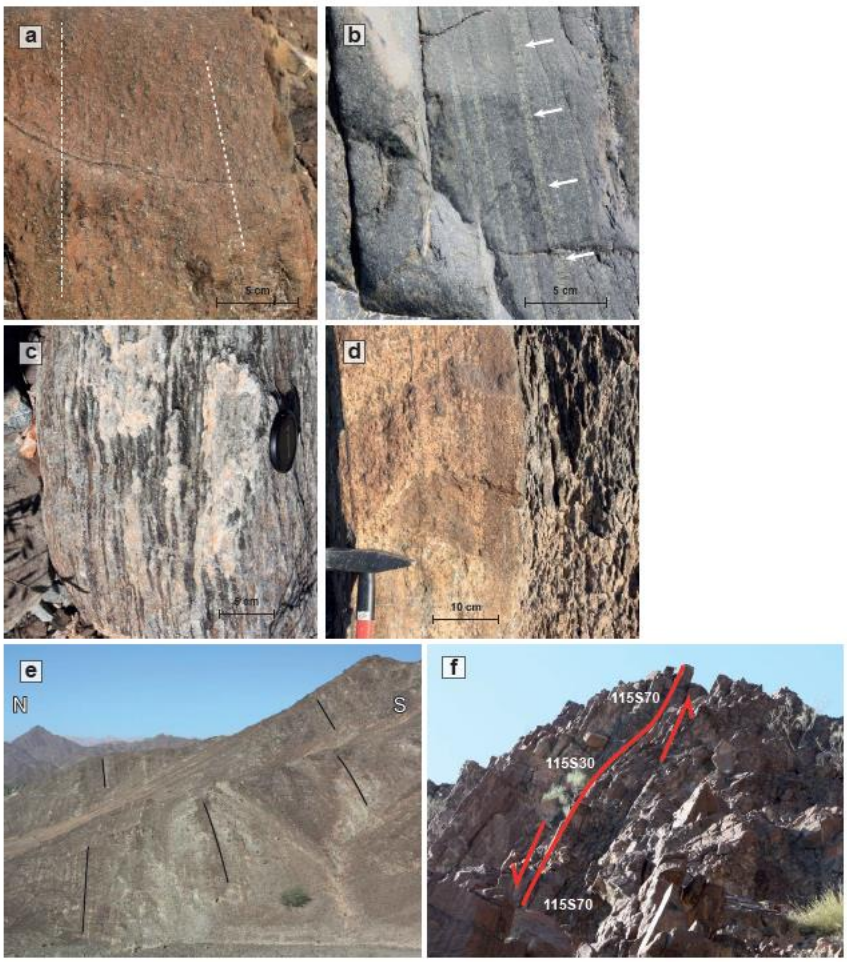

227

228 Fig. 2. Structures along the northern mantle-crust boundary affected by a high temperature normal
229 ductile shear zone. (a) Foliation in the porphyroclastic-submylonitic peridotite; (b) Highly stretched
230 pyroxenite banding in the mantle peridotite, the dashed lines showing vertical foliation planes; (c)
231 Gneissic structures in olivine gabbros from the lower crustal section, white bands rich in plagioclase
232 alternating with dark bands rich in olivine and pyroxene (N22°58'14", E57°20'10"); (d) Foliation in
233 deformed gabbroic (left) and ultramafic cumulates (right), underlined by a schistose parting in the
234 ultramafic interval (N22°58'52", E57°18'32"); (e) Progressive flattening of the cumulate layering to the
235 south, away from the mantle-crust boundary located a few hundred meters to the left of the photograph;
236 (f) Field evidence for a normal fault shear sense in the deformed lower crustal cumulates (N22°58'14",
237 E57°20'10").

238

239 The evolution of the intensity of the plastic deformation experienced by the lower crustal
240 cumulates is correlated with the dip of the layering which is sub-vertical (90°-80°S) along the
241 Moho, and tends to progressively flatten when moving south (Fig. 2e). The stretching lineation
242 is well developed and has a sub-vertical pitch (70° - 80°W to 80°E). The shear sense is normal
243 (down the dip), as revealed by macro-structural observations on the field (Fig. 2f) and

confirmed by a micro-structural study including lattice preferred orientation analysis (see section on EBSD data).

Along rare later shear zones parallel to the high temperature foliations, the deformed cumulates are partly transformed into greenschist facies minerals (epidote, chlorite, serpentine, and hydrogarnets associated with rodingitisation, pointing to temperatures comprised between 200°C and 400°C (Bach and Klein, 2007; Python et al., 2011).

4.1.3. The southwestern contact

The southwestern border of the lower crustal section is affected by a major strike slip mylonitic shear zone a few tens of meters in thickness (Fig. 3a). It has a minimum extent of 20 km along strike (in yellow on Fig. 1b), its central part being hidden by the quaternary deposits of wadi Bahla. This shear zone presents a slight but well-defined curvature, its strike rotating from NW-SE to WNW-ESE when moving from the NW to the SE. The mylonitic foliation is steeply dipping to the NE. The shear sense is essentially dextral. The stretching lineation, which is underlined by a well-developed pencil structure (Fig. 3b), has a moderate dip (20°-50° to the SE) pointing to a normal component to the movement.

A metamorphic gradient is observed along the strike of this shear zone, ranging from granulite-amphibolite facies at its intersection with the northern fault, at mantle depths, to greenschist facies when moving upsection to the SE. Along the northwestern part of the shear zone, the mantle peridotites are injected by gabbronoritic dykes that can represent 50% of the outcrop surface. Most dykes are deformed and adopt a flaser texture (Fig. 3c). Roundish porphyroclasts (0.1-1cm) of orthopyroxene (opx), clinopyroxene (cpx) and plagioclase (plg) are partly to completely recrystallized into a fine-grained matrix (<100 microns) with a mosaic texture. Brown amphibole is abundant in the recrystallized tails around the pyroxene porphyroclasts (Fig. 3c).

At the intersection between the northern normal fault and this shear zone, two generations of foliation and lineation can be measured: a ~135N50 foliation associated with a gently dipping lineation and a ~160SW70 one associated with a sub-vertical lineation. These rocks seem to have recorded the deformation of both the northern normal fault and of the southwestern shear zone. The detailed cross-cutting relationships between the EW fault and the NW-SE fault are obscured by felsic intrusions and quaternary deposits but it is clear that the EW fault cannot be

274 followed to the W of the NW-SE fault and that, at the contrary, the NW-SE fault persists to the
275 north beyond the EW fault.

Fig 3

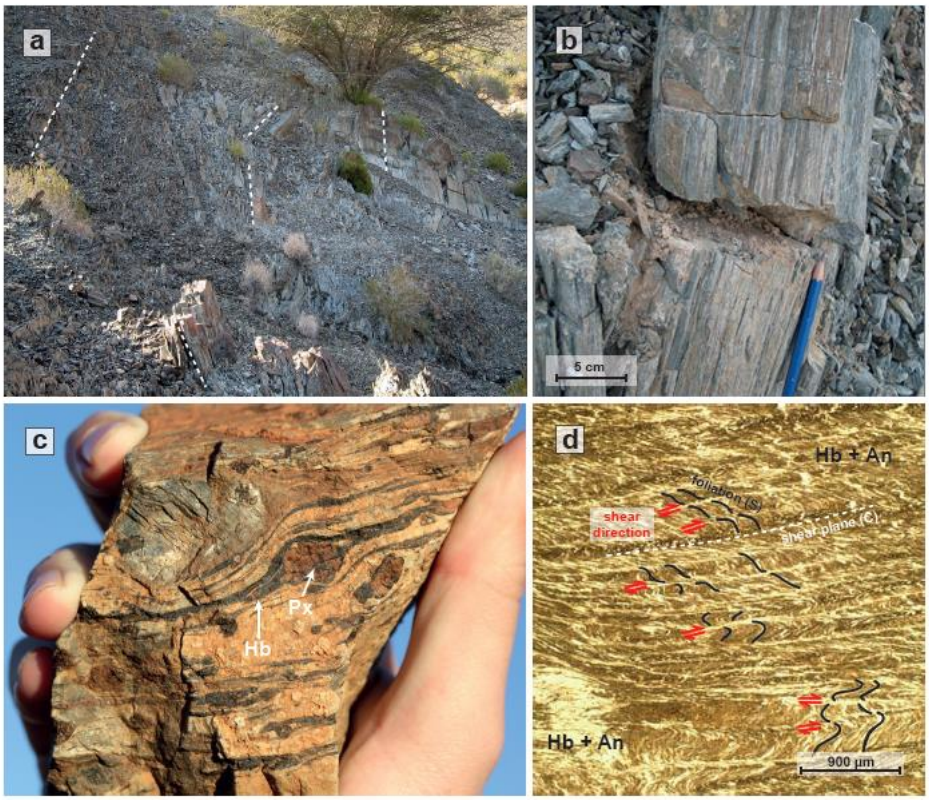

276

277 Fig. 3. Structures along the southwestern mantle-crust boundary affected by a mylonitic shear zone. (a)
278 General view, schistose parting and deformation orientation at local scale are highlighted by the white
279 dashed lines; (b) Detail on gabbro deformed and metamorphosed in the greenschist facies showing the
280 linear habit of the deformation (N22°59'14", E57°13'37"); (c) Deformed gabbronorite dyke showing a
281 flaser structure with hornblende (Hb) recrystallization tails around pyroxene (Px) porphyroclasts; (d)
282 Crenulations in the same gabbros (thin section in transmitted light, uncrossed Nicols), An: anorthite
283 plagioclase, Hb: hornblende (N22°57'36", E57°15'07").

284

285 Moving to the SE, the gabbros are still intensely deformed into mylonites and
286 ultramylonites. Structures include extreme stretching, sheath folds and crenulation cleavages
287 (Fig. 3d). Mylonitized gabbros transformed into plagioclase + hornblende are still present but
288 the assemblage chlorite + actinolite + tremolite typical of the greenschist metamorphic facies
289 becomes the more common. Porphyroclasts preserve intense intracrystalline deformation
290 (undulose extinction, bending and rotation associated with strain shadows, C/S shear bands).
291 The transition with the undeformed rocks is gradational. At its eastern termination, deformation
292 is partitioned into a swarm of thin cataclastic shear zones.

All along the shear zone, the high-temperature metamorphic mineral assemblages show a variable overprint of greenschist facies metamorphism with coronas of actinolite-tremolite around pyroxenes and recrystallization into tremolite, actinolite, chlorite, epidote, zeolite, prehnite, serpentine, talc and/or carbonate. Late veins of zeolite, carbonate, chlorite and serpentine commonly cut the mylonites.

4.1.4. The eastern contact

The contact between the mantle and the crustal section in the eastern part of the massif corresponds to a brecciated zone oriented NNW-SSE (in blue on Fig. 1b). Textures are cataclastic with large angular clasts of peridotite and gabbros embedded in a matrix essentially made of carbonate, serpentine, chlorite and prehnite (Fig. 4a and b).

Fig 4

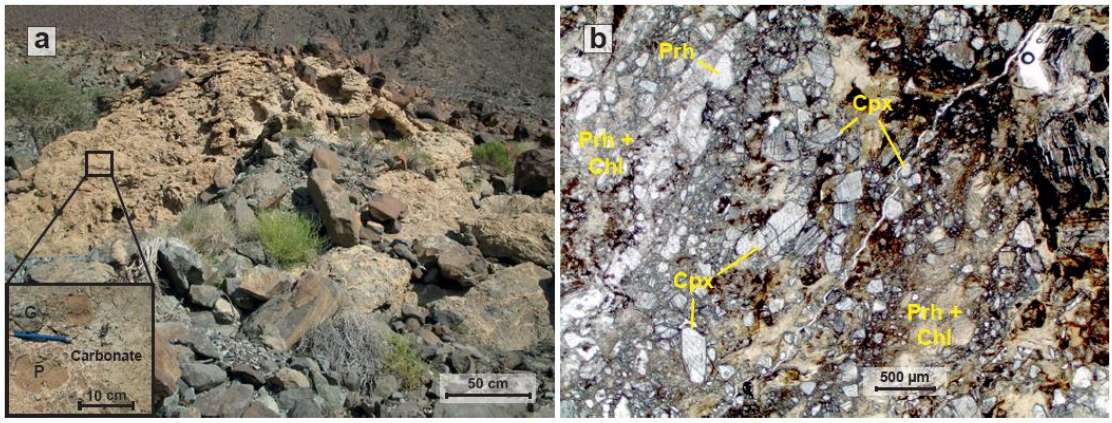

Fig. 4. Breccia with gabbroic clasts embedded in a carbonate-prehnite matrix typical of the eastern mantle-crust boundary (N22°54'53", E57°22'09". (a) General view, G: gabbroic clast, P: peridotite clast; (b) thin section view (in transmitted light, uncrossed Nicols), Chl: chlorite, Cpx: clinopyroxene, Prh: prehnite.

4.1.5. Flat-lying décollements

In the central part of the massif, not far from the city of Bahla, the mantle peridotites are overlain by a cap of layered gabbros presenting the same intense plastic deformation and the same sub-vertical orientation as the ones cropping out along the northern contact (Fig. 5a). The Moho at this site actually corresponds to a knife-cut sub-horizontal décollement gently dipping to the East (15°E). It is filled with fibrous chrysotile (Fig. 5b) and striated surfaces of carbonates.

Fig 5

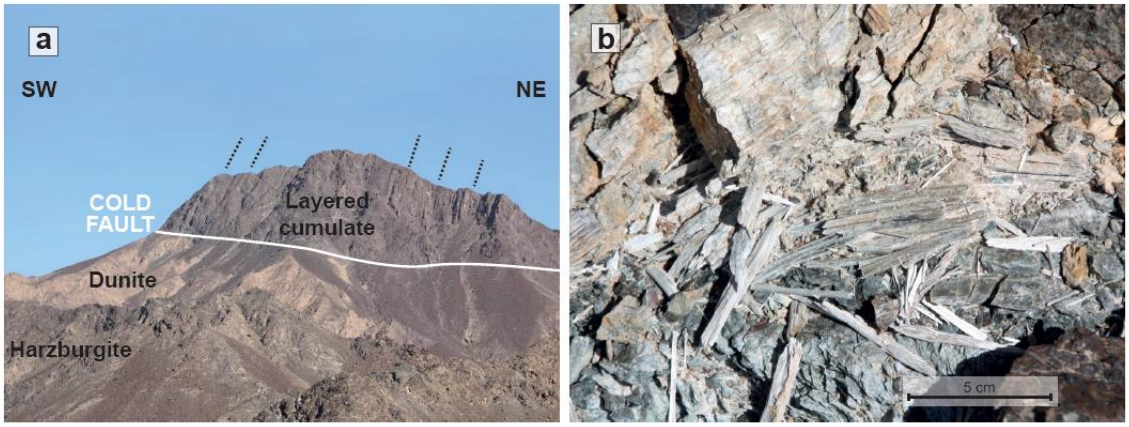

316

317 Fig. 5. Décollement (sub-horizontal "cold fault") at the mantle-crust boundary in the central part of the
318 massif (N22°57'42", E57°15'32"). Note the highly dipping (southward, dashed lines) deformed layered
319 gabbros at high angle to the faulted contact with the underlying transition zone dunites. (a) General
320 view; (b) Asbestos formation in the décollement.

321

322 4.2 Magmatic intrusions

323 4.2.1. Plagiogranite plugs and dykes

324 A few tonalite and trondhjemite intrusions elongated along the NNW-SSE direction and
325 up to several hundred meters in length intrude mantle harzburgites close to the intersection
326 between the northern normal fault and the southwestern shear zone (Figs. 1b and 6a, b). They
327 are made of plagioclase, quartz, and rare micas, (altered into chlorite) and amphibole. They are
328 intensely sheared with the development of boudinage (Fig. 6c) and of gneissic textures along
329 their margins with the NNW-SSE mylonitic shear zone while the internal part of the intrusions
330 is undeformed (coarse grained texture with no apparent mineral preferred orientation). This
331 deformation gradient is correlated with a mineralogical evolution: the felsic intrusions are more
332 tonalitic (i.e. richer in ferromagnesian minerals), with calcic plagioclase (An60-80) at the
333 contact with mylonitic peridotites while they are purely trondhjemitic (i.e. almost devoid of
334 ferro-magnesian minerals) with albitic plagioclase (An < 30) in the internal part of the
335 intrusions. Trondhjemitic dykes up to one meter in thickness inject the peridotites hosting the
336 major intrusions; some of them are affected by boudinage (Fig. 6b). One sample of trondhjemite
337 with a strong lineation from the intrusion pictured in figure 6a has been dated (U-Pb on zircon)
338 at 95.20114 ± 0.032 Ma (13211M02; Rioux et al., 2021a). This sample has an $\varepsilon_{Nd}(t)$ = -4.86
339 (Rioux et al., 2021b).

340

Fig 6

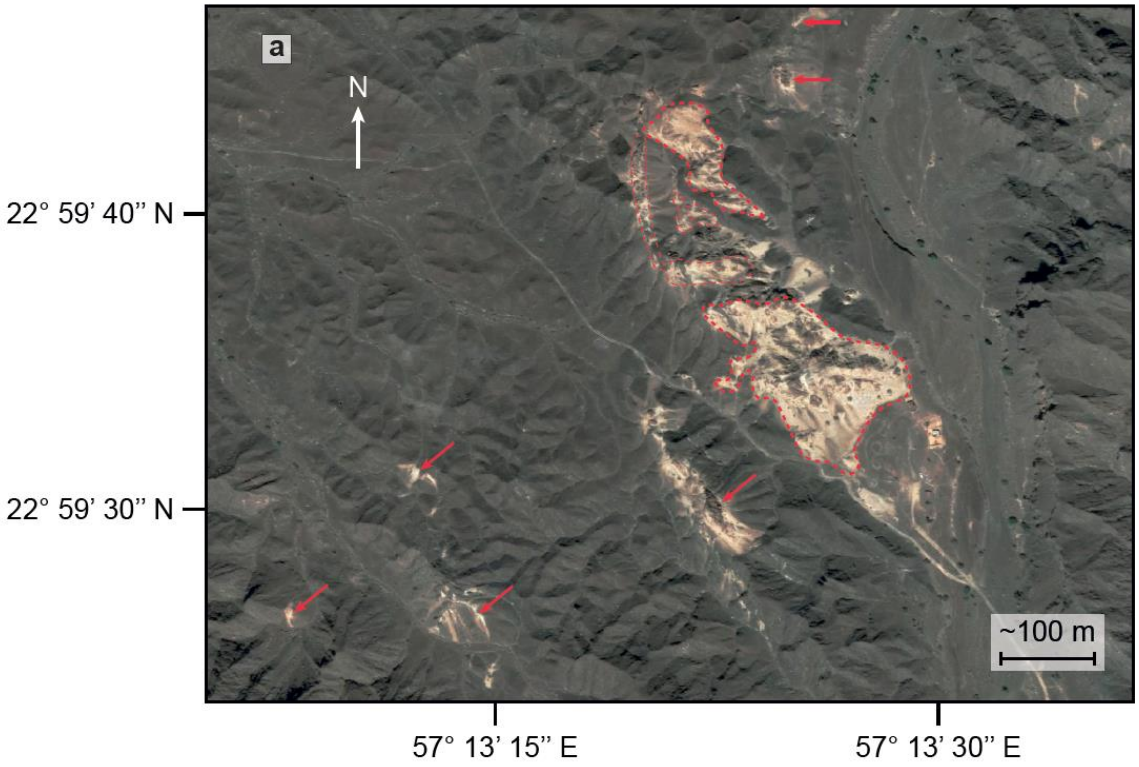

341

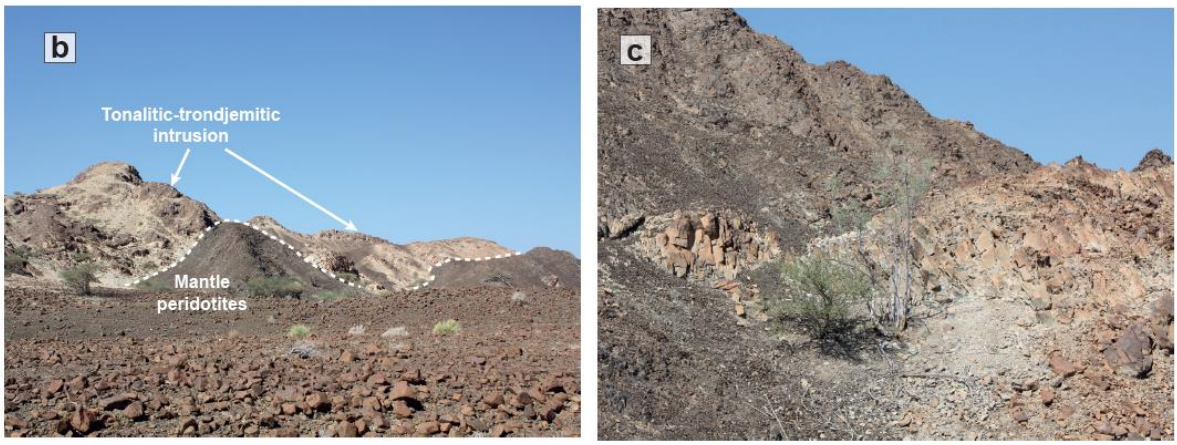

342

343 Fig. 6. Tonalitic-trondhjemitic intrusions (whitish outcrops) in mantle peridotite (brownish outcrops)
344 along the southwestern mylonitic shear zone. (a) Google Earth image showing the extent and the general
345 orientation (NW-SE to NNW-SSE) of these intrusions. The main outcrops of the largest intrusion are
346 highlighted by the red dashed lines, and smaller occurrences are shown by red arrows; (b) Outcrop view
347 on the main undeformed plug; (c) Deformed felsic dyke showing boudinage.

348

349

4.2.2. Post-tectonic olivine gabbro dykes

Along the northern contact, the deformed and tilted layered gabbros are intruded by a swarm of undeformed, discordant dykes a few decimeters in thickness (Fig. 7). They have a WNW-ESE direction and dip from 30° to 75° to the North, sharing a similar azimuth but having a different dip than the southward dipping deformed layered gabbros. They lack of chilled margins; some dykes show the development of coarse-grained margins (crescumulate textures). They are fine-grained olivine-gabbros having the composition of moderately evolved cumulates. Olivine has a Fo content (100 × molar $Mg/(Mg + Fe_{total})$) of about 77 mol% and a NiO content around 0.20 wt%, clinopyroxene an average XMg (100 × molar $Mg/(Mg + Fe_{total})$) of 83 mol% and average Cr_2O_3, Al_2O_3 and TiO_2 contents of 0.45 wt%, 2.4 wt% and 0.40 wt% respectively, and plagioclase an average An content of 87 mol%. The assemblage contains also minor amount of ferrichromite with an average XCr (100 × molar $Cr/(Cr + Al)$) of 55 mol%, YFe^{3+} (100 × molar $Fe^{3+}/(Cr + Al + Fe^{3+})$) of 43 mol% and an average TiO_2 content of 2.2 wt%. No orthopyroxene or igneous amphibole are present in these olivine-gabbro dykes.

Fig 7

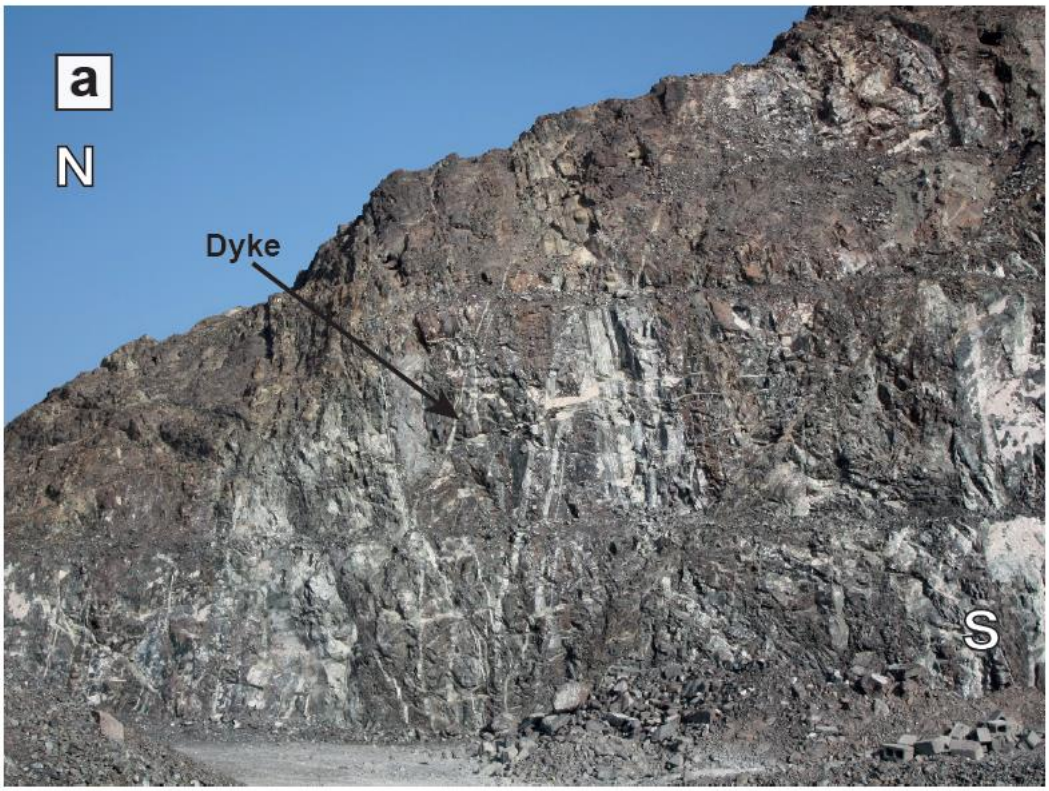

Fig. 7. Post-tectonic olivine gabbro dykes cross-cutting the deformed and tilted layered gabbros near the northern ductile fault.

4.3. Petrography of the layered cumulates

Our exhaustive sampling (210 samples) of the Bahla deformed and undeformed layered cumulates reveals an important lithological diversity in this unit. The layering of the crustal section results from the alternation of layers centimetric to pluricentimetric in thickness with different mineral proportions. The contrast between mafic and ultramafic layers is the more spectacular in the field, but microscope observations reveal more subtle variations in the modal content and textures. Following the classification of Irvine (1982) combining modal proportions and, when preserved, textural criteria for the crystallization order, seven main lithological groups can be defined in the layered cumulates of Bahla: troctolites, gabbros, opx-troctolites and gabbronorites for the mafic layers, dunites-wehrlites, clinopyroxenites and cumulate harzburgites for the ultramafic intervals.

It is worth mentioning that the so-called "wehrlite *intrusions"* invading the layered cumulates and present in most massifs of Oman (e.g. Juteau et al., 1988), are quite uncommon in Bahla and are thus not included in the present study.

- The **troctolites** (6% of the samples) are essentially adcumulate to mesocumulate cpx-troctolites; "pure" troctolites devoid of clinopyroxene (cpx) are uncommon. They essentially consist of euhedral to subhedral plagioclase (plg), subhedral olivine and interstitial to poikilitic cpx. The modal proportions are highly variable: the olivine content ranges from 5% to 70% and the cpx content from 0% to 20%. The modal proportion of plagioclase varies accordingly. A few troctolites also include traces (≤ 1%) of interstitial orthopyroxene (opx) and/or magmatic amphiboles. Chromian spinel is ubiquitous but generally not abundant (≤ 1%), reaching exceptionally 10%. Magnetite and sulfides can be present.

- The **gabbros** are the most common (61% of the samples) and principally consist of olivine-gabbros with variable modal proportions. They have the same petrographic characteristics and minor minerals as the troctolites, the difference between the two groups being the higher modal abundance of cpx and its subhedral to interstitial habit in the gabbros. Gabbros devoid of olivine (cpx and plg only) and anorthosites (>90% plg) do exist but are uncommon.

- The **opx-troctolites** (Fig. 8a) (12% of the samples) are characterized by the crystallization of opx and cpx slightly after plg and olivine. This is expressed by subhedral to

anhedral, sometimes poikilitic, pyroxenes (up to 37% of opx and 15% of cpx) associated with euhedral to subhedral plg (24% - 87%) and subhedral olivine (5% - 49%). They have ad- to orthocumulate textures (> 25% of post-cumulus material). The main opaque mineral phase is magnetite, which is not abundant (≤ 2%) and is rarely associated with sulfides and chromian spinel. Magmatic amphiboles are common in these troctolites; they are mostly interstitial with modal proportions of less than 3%. This, together with the paucity of chromian spinel, contrasts with the troctolites and olivine-gabbros.

- The **gabbronorites** (5% of the samples) occur as layers alternating with other mafic lithologies in the layered cumulates. They are medium-grained adcumulates characterized by the early crystallization of opx (cumulus phase). They present euhedral to subhedral crystals of opx (10% - 47%) and plg (30% - 75%) and always subhedral cpx (5% - 25%). When olivine is present (olivine-gabbronorite), it is subhedral to anhedral and variably abundant (2% - 25%). Only a few samples contain opaque minerals (<1% of chromian spinel and/or magnetite).

- The **clinopyroxenites** (2% of the samples), alternating with mafic layers, are coarse-grained mesocumulates and orthocumulates characterized by abundant (60% - 92%) euhedral to subhedral cpx and interstitial post-cumulus olivine, plg and/or opx; no "pure" clinopyroxenite is observed. Olivine is the most abundant post-cumulus phase (7% - 38%) while plg and opx have modal proportions ranging from 1% to 8%. Chromian spinel is observed in some clinopyroxenites.

- The **dunites-wehrlites** (13% of the samples) appear as layers alternating with gabbros. They are medium to coarse-grained adcumulates and mesocumulates. Dunites are essentially composed of euhedral to subhedral olivine (≥ 85%) and usually present poikilitic plg. Chromian spinel is present in the rare "pure" dunites only and can be abundant (up to 10%). Wehrlites are made of olivine (32% - 92%) and cpx (2% - 42%). Olivine is a euhedral to subhedral cumulus phase. Cpx is a post-cumulus, often poikilitic, phase. Post-cumulus plg and opx are common as interstitial or poikilitic crystals and can be relatively abundant with modal proportions varying from 5% to 33% for plg and from 6% to 22% for opx. Opaque minerals include chromian spinel, magnetite and minor sulfides. Their abundance varies from 0.5% to 6%.

- The **harzburgites** (Fig. 8b) (1% of the samples) are medium-grained orthocumulates characterized by rounded or subhedral cumulus olivine (38% - 48%) and post-cumulus opx, cpx and plg. Opx is abundant (15% - 32%) and appears generally as large (2-5mm) subhedral poikilitic crystals including numerous rounded olivine. Poikilitic plg and cpx constitute the rest

of the mineral assemblage. Cpx is present as both small (≤ 1mm) subhedral to anhedral grains and larger poikilitic crystals. This texture indicates that opx crystallized slightly before cpx and that plg was the last phase to crystallize. Minor (≤ 1%) subhedral chromian spinel and pleonaste are common. It is worth mentioning that cumulate harzburgites, cropping out as weathered low hills on the southern border of the Bahla massif, are mapped as mantle peridotites in geological maps. We realized lately that these rocks adopted a cumulate texture and were actually part of the crustal section. Accordingly, the abundance of cumulus harzburgite is certainly much higher than the 1% estimate based on our sample proportions.

Fig 8

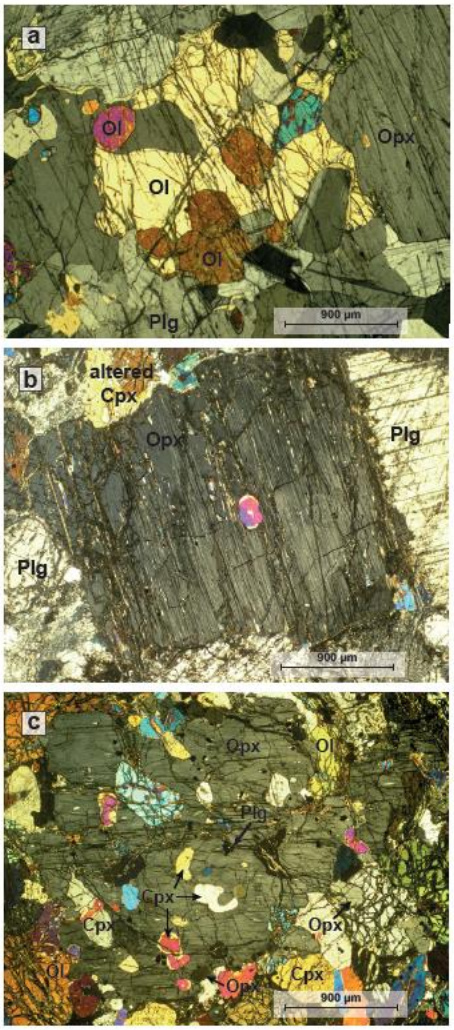

Fig. 8. Igneous facies in the undeformed lower crustal cumulates. (a) Opx-troctolite (sample 08BA8Fb ZII); (b) Subhedral opx crystal in an opx-troctolite (sample 09BA14 ZI; N22°54'26", E57°19'50"); (c) Cumulate cpx-harzburgite with poikilitic opx (sample 09BA14 ZI).

444 4.4. Microstructure and mineral fabric of deformed cumulates

445 Crystallographic preferred orientation (CPO) of olivine, pyroxenes, and plagioclase have
446 been measured using Electron Backscatter Secondary Diffraction (EBSD) in 5 samples from
447 the northern contact including 1 troctolite, 3 gabbronorites, 1 olivine-gabbronorite (Fig. 9).

448 Where olivine is present, its [100] axes are at low angle to X and [010] are sub-
449 perpendicular to the foliation plane (XY) suggesting the activation of the classical [100](010)
450 A-type slip-system (X and XY are respectively the lineation and foliation deduced from the
451 mineral flattening and elongation and from the shape preferred orientation). The A-type slip
452 system is usually interpreted to be formed at high temperature, low stress and dry conditions
453 (Nicolas et al., 1971; Ben Ismail and Mainprice, 1998; Karato, 2008).

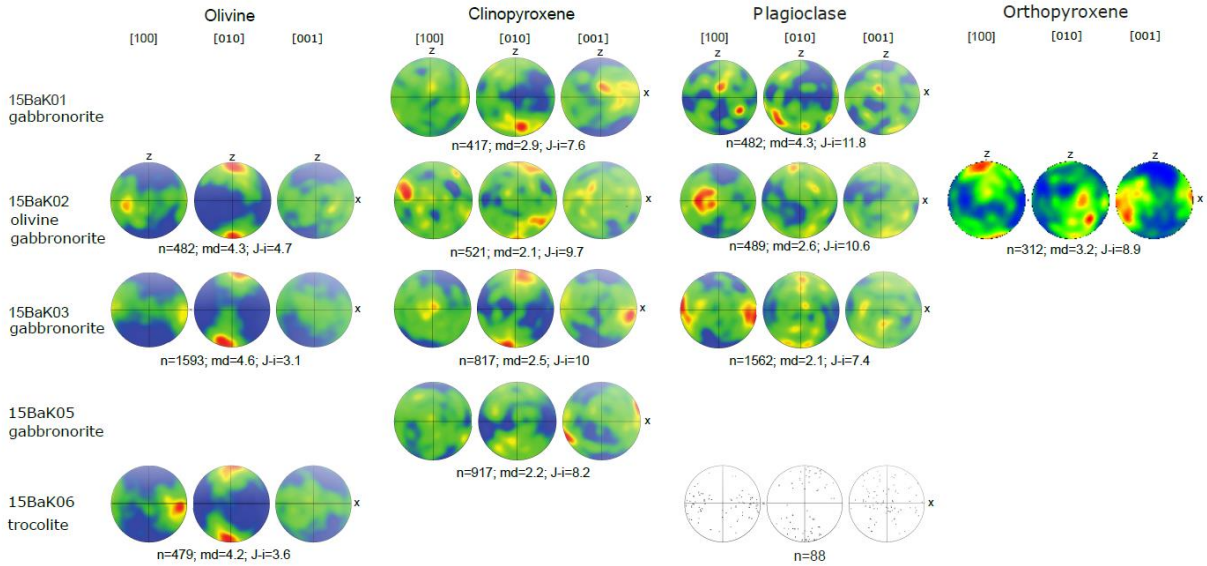

454

455 Fig. 9. Crystallographic preferred orientation of olivine, clinopyroxene, plagioclase and orthopyroxene
456 from five samples. Poles figures represent one point per grain on a lower-hemisphere, equal area
457 stereographic projection; N is the number of grains, md is the multiple of uniform distribution, which is
458 calculated for pole figures with more than 110 grains. The strength of the crystallographic preferred
459 orientation (CPO) was estimated using the J-index (Bunge, 1982).

460

461 Clinopyroxene shows [001] or [100] axes sub-parallel to the lineation and parallel to
462 olivine [100] axes, and [010] axes sub-perpendicular to the foliation plane.

463 Plagioclase presents CPO patterns where [100] axes show a point concentration sub-
464 parallel to X, and weak concentration of [010] axes sub-parallel to Z, suggesting the possible

activation of the [100](010) slip system which is the dominant activated slip system in plagioclase (Marshall and McLarent, 1977; Olsen and Kohlstedt, 1984) at temperature higher than 700°C (e.g., Diaz Aspiroz et al. 2011, Kruse et al. 2001).

Orthopyroxene has been observed in one sample (15BaK02). The pattern displays point concentrations of [001] axes sub-parallel to X and of [100] axes sub-parallel to Z, suggesting the activation of [001](100) slip system, known to be activated at high temperature (e.g. Ross and Nielsen, 1978).

The alignment of olivine [100] axes, clinopyroxene [001] or [100] axes, plagioclase [100] axes, and orthopyroxene [001] axes sub-parallel to the stretching lineation (X) suggests coeval deformation of these minerals. In detail, these crystallographic axes display a small angle to the stretching lineation which, combined with the orientation of the foliation (sub-vertical to high southward dip bearing a vertical lineation), (where X represents the top of the outcrop) confirm the normal shear sense determined on the basis of macroscopic field criteria.

4.5. Mineral chemistry of the layered cumulates

4.5.1. Major and minor elements (Supplementary Table 1)

Pyroxenes from the lower crustal cumulates are diopsides ($Wo_{45-52}En_{44-51}Fs_{2-10}$), magnesium-rich augites ($Wo_{41-45}En_{46-53}Fs_{5-10}$) and enstatites ($Wo_{0-5}En_{73-90}Fs_{9-24}$), and are characterized by low-aluminium contents (average $Al_2O_3 \approx 2.1$ wt% in cpx and 1.2 wt% in opx). Their XMg (calculated with total iron) vary from 80 to 95 mol% for cpx and from 76 to 89 mol% for opx. Similarly, the forsterite (Fo) content of olivine and the anorthite (An) content of plg present wide compositional ranges varying from 76 to 89 mol% and from 67 to 99 mol% respectively.

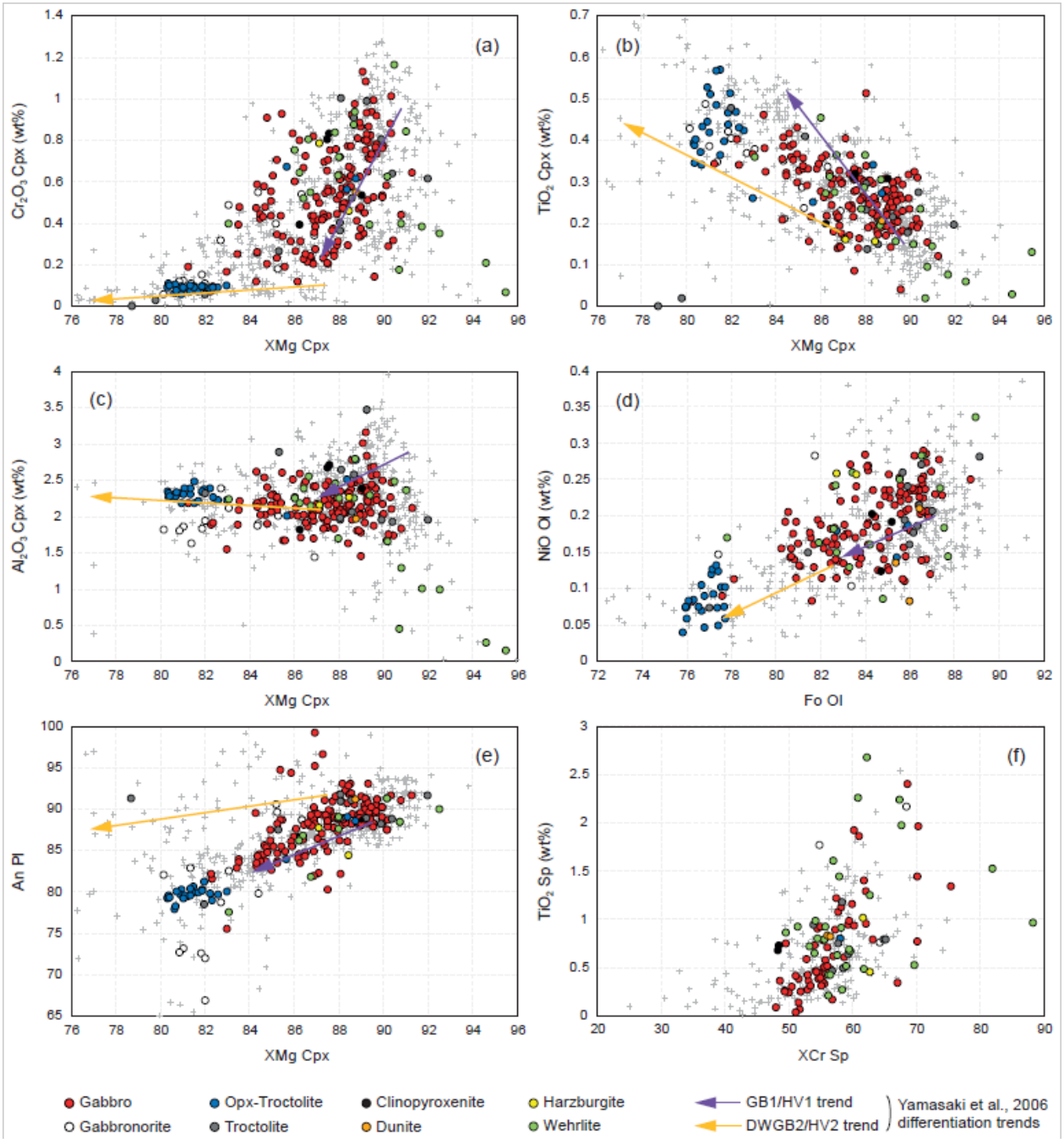

Fig. 10. Major and minor elements content determined on minerals with the electron microprobe. Crosses: data on lower crustal cumulates from other massifs of the Oman ophiolite (Abily, 2011, Korenaga and Kelemen, 1997; Müller, 2015; Yamasaki et al., 2006). Each dot and cross represents the average values for one sample.

In terms of classical differentiation indexes (Fo and Ni in olivine, An in plagioclase, XMg, Cr_2O_3 and TiO_2 in pyroxenes), the mafic and ultramafic cumulates of Bahla range from primitive to moderately evolved and plot in the field of other Oman ophiolite lower crustal cumulates (Fig. 10a, b, c). Relatively evolved compositions (XMg_{cpx} < 83 mol%, XMg_{opx} < 79 mol%, Fo < 78 mol%, An < 82 mol%) are observed in opx-troctolites and in gabbronorites. These relatively evolved cumulates are also characterized by high titanium contents in cpx (TiO_2 > 0.80 wt%), low chromium contents in pyroxenes and low NiO contents in olivine, close or below the detection limits.

In other terms, most opx-troctolites, part of gabbronorites and rare gabbros, one troctolite and one wehrlite, define a distinct group at the most evolved end of the general trend. This is particularly evident in the composition of olivine which shows a clear compositional gap in Fo between between 80 and 78 mol%, perfectly correlated with its NiO content (Fig. 10d). This hiatus is likely not an artefact of sampling as (1) the number of samples is statistically significant (> 200 samples), (2) they cover a large lithological diversity, i.e. it is unlikely that we missed some facies corresponding precisely to this differentiation index, and (3) we sampled the different parts of the massif and different stratigraphic levels. This dichotomy is also reflected in both cpx and opx compositions (Fig. 10a, b, c) and in the plagioclase composition (Fig. 10e). The Al content of pyroxenes does not show any correlation with lithology, apart from a few dunites and wehrlite showing a "abnormally" low Al content (and to a lesser extent in Cr) in pyroxenes (Fig. 10c) given their high XMg. This likely reflects the impact of high temperature hydrothermal processes (cf. Python et al., 2007, 2011; Rospabé et al., 2017).

Within the most primitive group, Fe-Mg phases and plg in gabbros have globally the same range of composition for major (XMg, Fo, An) and minor (TiO_2, Cr_2O_3, NiO) elements than those in the dunites-wehrlites (Fig. 10). However, the high-XMg cpx (XMg > 92 mol%) crystallized preferentially in dunites-wehrlites while the high-calcium plg (An > 94 mol%) are only observed in gabbroic cumulates. Troctolites, harzburgites and clinopyroxenites plot in the same compositional field as the one of dunites-wehrlites and gabbros. However, troctolites have generally more primitive compositions ($XMg_{cpx} \approx$ 89 mol%, Fo ≈ 86 mol%, An ≈ 90 mol%) than those of cumulate harzburgites and clinopyroxenites ($XMg_{cpx} \approx$ 88 mol%, Fo ≈ 84 mol%, An ≈ 88 mol%).

Yamasaki et al. (2006) identified two suites in the Oman layered crust based on distinct trends in their clinopyroxene composition: GB1/HV1 which has composition consistent with a

MOR-related setting, and DWGB2/HV2 that was attributed to a SSZ setting. In comparison, we can see that the Bahla cumulates follow a trend closer to the GB1 suite (e.g. An vs. XMg cpx) or intermediate between those two trends (e.g. TiO2 vs. XMg cpx).

The XCr in Cr-spinel ranges from 50 to 70 mol% with a few outliers toward high Cr. Their TiO_2 content presents huge variations, from virtually zero to almost 3 wt% (Fig. 10f). No correlation is observed between the Cr-spinel composition and the lithology, although Cr-spinel is absent from the most evolved cumulates in which the main opaque mineral is usually magnetite.

The most evolved cumulates (XMg_{cpx} < 85 mol%) crop out essentially in the east and in the southeast of the main crustal section and belongs to both layered and overlying more "massive" (i.e. with no ultramafic layers making the layering evident in the field) cumulate units. The most primitive cumulates (XMg_{cpx} > 89 mol%) are principally observed along or close to both the high-temperature and the low-temperature faults. The "massive" cumulate unit is mainly composed of relatively evolved cumulates.

4.5.2. Trace elements in cpx (Supplementary Table 2)

Cpx in cumulates of all lithological groups have similar shape of chondrite-normalized Rare Earth Elements (REE) patterns (Fig. 11a), characterized by a depletion in Light Rare Earth Elements (LREE) compared to Middle and Heavy REE (MREE-HREE; nearly flat segment from Gd to Lu) and by the lack of Eu anomaly. Their chondrite-normalized La/Yb ratios vary from 0.03 to 0.11. The REE contents of cpx range from 10^{-1} (LREE) to 10 times (HREE) the chondritic values. The most enriched cpx are essentially observed in in opx-troctolites and gabbronorites, one opx-troctolite and one ol-gabbro while the most depleted cpx are preferentially observed in some (ol-)gabbros, troctolites and dunites-wehrlites, which is consistent with variations in incompatible minor elements.

Primitive mantle-normalized extended trace elements patterns of cpx in all lithological groups (Fig. 11b) are characterized by depletion in the most incompatible elements. For more compatible elements (Nd - Lu segment), all patterns have a similar shape characterized by a strong negative anomaly in Zr (Zr/Sm_{PMN} = 0.15-0.35) and Hf and a less pronounced negative anomaly in Ti (Ti/Gd_{PMN} = 0.53-0.80) relative to neighbouring REE. The amplitude of Ti anomaly (i.e. more variable Ti/Gd_{PMN}) is slightly higher in cpx of gabbronorites and in one opx-troctolite and one ol-gabbro (Ti/Gd_{PMN} < 0.6). Conversely, for most other incompatible trace

elements (Rb - Sr segment), patterns are quite intricate and overlap each other. A clear negative Sr anomaly is observed in most samples and its amplitude generally increases with the increase in the Ti content (i.e. stronger anomalies in some gabbronorites, opx-troctolites and gabbros, with Sr/Nd ratios mostly < 0.4). However, in some trace element patterns, this negative Sr anomaly is weaker (samples with the lowest REE and Ti contents); cpx in all dunites-wehrlites and troctolites present this characteristic. Similarly, a clear negative Nb anomaly of varying amplitude is observed in most patterns, with stronger anomalies in patterns displaying the stronger negative Ti anomalies. Apart for these light tendencies, the presence and the amplitude of all trace element anomalies are largely independent of the lithological group with large variabilities even in a single lithological group (especially the (ol-)gabbros).

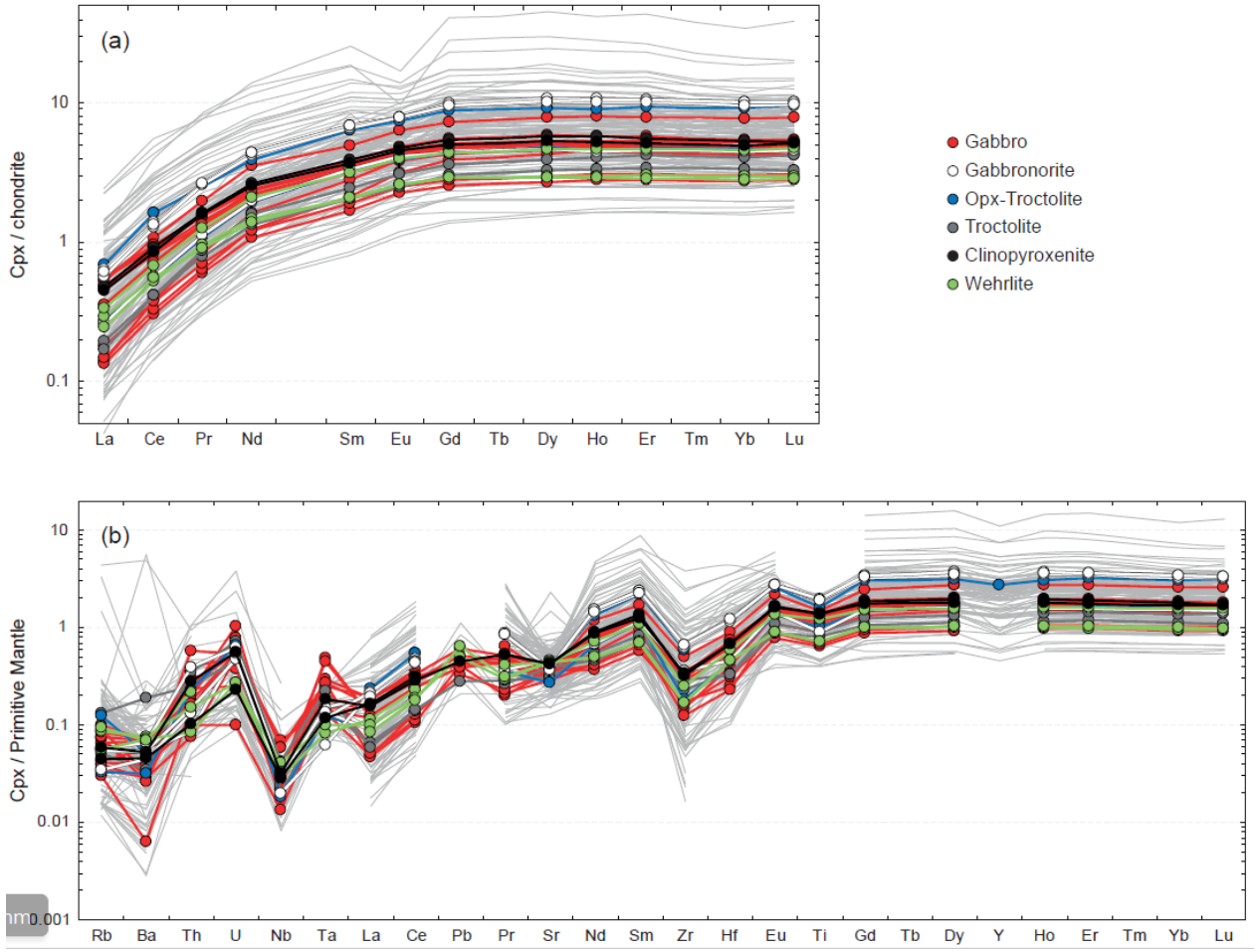

Fig. 11. Trace elements content of clinopyroxene determined with LA-ICP-MS. Grey lines: data on lower crustal cumulates from other massif of the Oman ophiolite (Abily, 2011, Korenaga and Kelemen, 1997; Müller, 2015; Yamasaki et al., 2006). Each pattern represents the average values for one sample. Symbols as in Figure 10.

575 5. Discussion

576 5.1. Structural specificity of the Bahla massif.

577 Our survey has revealed that several structural features of the Bahla massif contrast with
578 common views concerning the Oman ophiolite. Among these paradigms, the lower crustal
579 section of Semail is generally described as a laterally continuous unit and the layering of the
580 basal cumulates is considered as parallel or at low angle to the mantle-crust boundary, equated
581 with the paleo-horizontal plane (cf. Pallister and Hopson, 1981). Clearly, the Bahla massif is an
582 exception to the rule for these aspects. The present general shape and size of its plutonic section
583 - a 15 by 8 km ellipsoid in map view - is clearly not attributable to the erosion of a former
584 laterally continuous crustal unit conformably resting on the underlying mantle peridotites. It is,
585 at least partly, a more pristine characteristic of this massif inherited from the interplay of a few
586 major fault zones that recorded different kinematics and were active over a wide temperature
587 range, during the accretion of the ophiolite and the early stages of intra-oceanic thrusting or
588 nascent subduction.

589 On the geological maps and associated structural sketches of the area, the apparently
590 dismembered aspect of the Bahla massif is attributed to the same tectonic events responsible
591 for the regional faulting and folding of the nearby autochthonous and allochthonous
592 sedimentary formations (Wyns et al., 1992; Béchennec et al., 1992). While we cannot exclude
593 *a priori* that the late décollements and cataclastic breccia correspond to such late tectonism, the
594 high temperature ductile faults we described above were active much earlier. As a matter of
595 fact, in this external part of the Northern Oman Mountains, the sedimentary formations escaped
596 any high temperature history, apart from a moderate, very low temperature imprint of upper
597 anchizone metamorphism (Breton et al., 2004). On the other hand, the seemingly synclinal-like
598 geometry of the Bahla massif was, among other arguments deduced from the occurrence of the
599 mantle section along both the northern and the southern contacts with the crustal section. We
600 realized that, to the south, the peridotites were mostly ultramafic cumulates, part of the crustal
601 section and cannot be used as an evidence of general folding of the Bahla massif.

602 5.2. The Moho at Bahla: a major syn-magmatic normal fault.

603 The highest temperature tectonic contact between the mantle and crustal sections we
604 identified in Bahla is a ductile normal fault of lateral extent exceeding 15 km and striking
605 WNW-ESE, at low angle to the direction of the former ridge axis. It is interrupted to the west
606 by a lower temperature shear zone and to the east by a brittle fault. The deformation textures

and the lattice fabrics, together with the preservation of the magmatic igneous mineral assemblage - apart from the local and partial transformation of the pyroxenes into metamorphic amphibole - point to very high temperature conditions during deformation, close to the gabbro solidus.

High temperature conditions during deformation is attested by the activation of the high temperature slip systems in olivine and pyroxenes. It is confirmed by thermometric determinations (Supplementary Table 3). Temperatures have been estimated for orthopyroxene and clinopyroxene using Brey and Köhler (1990) thermometer (Opx_{BK90}) based on Ca contents in opx, and two-pyroxenes Brey and Köhler (1990) thermometer ($2Prx_{BK90}$) based on Fe–Mg exchange (see table in supplementary material). These thermometers have been applied at a pressure assumed to be 0.2 GPa, implying equilibration in the plagioclase stability field. Both thermometers have been applied on all types of gabbro, which have been classified for these calculations by the apparition of orthopyroxene during the crystallization sequence. The first group concerns gabbro with early crystallization of orthopyroxene (5 samples), the second group where orthopyroxene and clinopyroxene crystallized simultaneously (8 samples), and the third group where the orthopyroxene is late in the crystallization sequence (12 samples). For all groups, the estimated temperatures are similar giving an average temperature of 984 ± 44 ˚C and 920 ± 47 ˚C using Opx_{BK90} and $2Prx_{BK90}$ thermometers respectively. The two pyroxenes thermometer is always slightly lower in temperature but within the range of Opx_{BK90}. In details, there is no temperature difference within the three identified groups of orthopyroxenes.

Almost monomineralic thin bands of anorthosites are common features in these deformed gabbroic cumulates. They can reflect segregation processes during deformation of a crystal mush (e.g. Abily et al., 2011) and would be evidence of incomplete crystallization of the lower crust when the shearing initiated. They could also represent metamorphic segregations at high temperature in the solid state. The good preservation of the igneous layering, i.e. the alternation of decimetres-thick mafic and ultramafic cumulate layers, in spite of the intensity of the deformation, could be inherited from the initial strain partitioning in the layers richer in interstitial melt. The formation of the layering itself may be contemporaneous with the early stage of deformation. Once fully crystallized, the sub-solidus plastic deformation affected the cumulates and adjacent mantle peridotites in a more homogeneous way, but the initial focusing of the ductile normal fault at Moho level is inherited from and earlier, probably syn-magmatic stage.

Field observations and oblique lattice fabrics relative to the foliation and lineation point to simple shear deformation. It allows us to determine a shear sense and to confirm the down the dip displacement of the crustal section relative to the mantle section, primarily deduced from field arguments. A normal fault sense is also consistent with the polarity of the rotation of the gabbro layering away from the fault, i.e. flattening to the south. The important steepening of the layering of the cumulates as the fault is approached was clearly induced by the same tectonic event as the one that imprinted the plastic deformation, given the correlation between the dip of the layering and the deformation intensity.

This "tectonic Moho" is presently sub-vertical. However, the Bahla massif presents a general tilt of about 20° southward, induced by the post-obduction doming of the nearby Jebel Akhdar; it is reflected, among other, in the dip of the cumulate layering away from the fault. Accordingly, it seems reasonable to infer that the original dip of the northern fault at the time it formed at the spreading centre was closer to about 70°S. Here again, this reconstruction is consistent with a normal fault leading to the downward displacement of the layered gabbro relative to the mantle peridotites. This displacement was likely substantial, even if impossible to quantify, given the deformation intensity and the thickness of the zone of affected by plastic deformation.

The activity of the fault ceased before cooling below the brittle–ductile transition of the cumulates, as attested by the moderate imprint of low temperature deformation, limited to some serpentine shear zones focused mainly in the ultramafic cumulate layers and preserving the flaser structure of the gabbros. Moreover, there is clear evidence that the tilt of the gabbro, and thus the normal fault activity, is prior to the end of the igneous activity in the Bahla massif, as attested by the occurrence of dykes cross-cutting the deformed cumulates. These dykes are parallel to the azimuth of the former ridge axis and filled with a mineral assemblage (olivine gabbro) consistent with derivation from a moderately evolved MORB-like tholeiite. The presence of crescumulate textures on the inner walls of several of these dykes together with the absence of chilled margins indicate that the cumulates slightly, but not extensively cooled down at the time of injection ($T° >> 400°C$).

5.3. The southwestern shear zone as a high temperature trans-tensional ductile fault.

The style and geometry of the southwestern NW-SE fault contrasts markedly with the one of the northern fault: its thickness is much less (tens of meters compared to hundreds of meters);

the deformation conditions do not exceed amphibolite facies; mylonitic textures are the rule; the overprint of greenschist facies and cataclastic deformation is more widespread.

The kinematics is the one of a dextral strike-slip shear zone with a moderate down the dip component. The deformation fabric is very linear, with a well-defined stretching lineation. Consistently, the dip of the foliation is quite variable, ranging from high to moderate northward. If we consider the 20°S general tilt of the massif, it can be inferred that the average original dip of the fault plane was closer to 45°N toward the axis. Combined with the moderate dip of the lineation southward and with the dextral shear sense, this geometry is consistent with that of a transtensional ductile fault.

In contrast to the northern fault where the deformation plane is parallel to the igneous structures, this mylonitic shear zone cross-cuts the bedding of the gabbros. The observed metamorphic gradient from high temperature at the NW termination of the fault, where it roots in the mantle section, to colder conditions to the SE, likely results from the fact that shallower levels of the crust are progressively encountered when moving to the SE. Accordingly, it would not reflect a real along strike metamorphic gradient at a constant depth.

This shear zone was active during and after intense magmatic injection. The lithological nature of these intrusions contrasts with those of the bulk of the crust: these are essentially pegmatitic gabbronorites and tonalite/trondhjemite dykes and plugs. Most of the dykes are intensely deformed, including the felsic ones. The largest felsic plug is located where the northern fault is interrupted by the mylonitic shear zone. It is free of shearing except along its margins. This is consistent with the transtentional nature of the movement which made room for the emplacement of the plug. These structural observations together with the age (95.201 ± 0.032 Ma) confirms the fact that the emplacement of felsic melts at near Moho depth, and thus the faults activity, occurred early and was nearly contemporaneous with the average accretion age of the Semail ophiolite determined at the global scale. The $\varepsilon_{Nd}(t)$ of -4.86 determined for this plug reveals a sedimentary component in its source (Rioux et al., 2021b) suggesting that this final magmatic episode and the late activity of the mylonitic faults were contemporaneous with the intraoceanic thrusting. The position of the Semail basin close to the continental margin could account for the presence of sediments in an environment of ocean crust generation.

5.4. Low temperature, but maybe not late décollements and breccias.

In restricted parts of the Bahla massif, the peridotite-gabbro contact adopts a sub-horizontal attitude but this is clearly a consequence of a low temperature décollement. The high angle between the deformed gabbros layering and the contact contrasts with the situation in most other massifs of Oman. Elsewhere a sub-horizontal paleo-Moho, parallel to the bedding of the lower crustal cumulates, is the rule and evidently a pristine feature (e.g. Boudier and Nicolas, 1995), although locally affected to some degree by faulting over a wide temperature range (Glennie et al., 1973; Abily et al., 2011; Zihlmann et al., 2018; Rospabé et al., 2019). In Bahla, these contacts are underlain by rodingites and diopsidites, together with the presence of chrysotile, indicative of temperatures exceeding the regional upper anchizone metamorphic conditions affecting the sedimentary formations near Bahla (Breton et al., 2014). Breccias with gabbroic elements embedded in a matrix of prehnite and carbonates are definitely lower temperature features but their occurrence is frequent in fault zones affecting the lower crust and the mantle along present-day mid-ocean spreading centres (e.g. MacLeod et al., 2002; Gillis et al., 2014) and arc related basins (e.g. Harigane et al., 2011) . Accordingly, although it cannot be strictly demonstrated, the fact that these relatively low temperature brittle faults predate the obduction and belong to the same tectonic episode than the high temperature faults of Bahla is in the field of possibilities. The preservation of greenschist facies and higher temperature alteration minerals in these breccias in spite of lower temperature overprint is, however, a good indication that they developed early.

5.5. Petrological specificity of the Bahla lower crustal layered cumulates.

Our exhaustive sampling of the lower crustal cumulates of the Bahla massif has revealed the important lithological diversity of this unit. It includes most rock types described up to now in other massifs of Oman and, in addition, lithologies that, as far as we know, seem more specific to this frontal part of the ophiolite i.e. the cumulate harzburgites and the opx-troctolites.

Orthopyroxene appears more abundant and ubiquitous in the lower crustal cumulates at Bahla than elsewhere in Oman, at the massif scale at least: 41% of our samples present post-cumulus opx and 17% early crystallizing opx (cumulus or early post-cumulus). These are minimum values as we under-sampled the cumulate harzburgites. Early crystallizing orthopyroxene is virtually absent from the lower crustal cumulates of entire massifs, especially in the southern part of the ophiolite (e.g. Pallister and Hopson, 1981; Kelemen et al., 1997) and present but more occasional than in Bahla in some sections of other massifs, mostly in the central and northern part of the ophiolite (e.g. Smewing, 1981; Browning, 1990; Yamasaki et

al., 2006; Abily, 2011). This abundance in early crystallizing orthopyroxene is thus another distinctive characteristic of the Bahla massif that might be shared with the nearby Wuqbah massif cropping out also at the front of the ophiolite (Abily, 2011).

A simple way to account for the early crystallization of orthopyroxene in an ocean spreading context is to invoke a parent melt with a silica content a few percent higher than in MORB, i.e. with a more andesitic composition, or an increase of the partial pressure of water and/or the oxygen fugacity in the melt, the two hypotheses being not mutually exclusive. The origin of the water or of the water-rich melts can be looked for in the subduction factory (e.g. MacLeod et al., 2013; Belgrano and Diamond, 2019; Koepke et al., this volume) or in deep-seated episodic hydrothermal processes in a spreading ridge context (e.g. Benoit et al., 1999; Boudier et al., 2000; Nonnotte et al., 2005; Rospabé et al., 2017).

Primitive or moderately evolved opx-rich lithologies (pyroxenites and gabbronorites) are the dominant facies in the dykes cross-cutting the mantle section of Bahla showing that, at a certain stage, it was percolated by andesitic, hydrous melts (Fig. 1b and Python and Ceuleneer, 2003). We can guess that these melts contributed to feed the crustal magma chamber. This would be consistent with the high proportion of opx-rich cumulates at Bahla. It is worth mentioning that, in the Oman plutonic section, orthopyroxene can be abundant in highly evolved cumulates but, in these cases, it has a low XMg and generally co-crystallizes with Fe-Ti oxides, amphibole and, occasionally, sulfides. This was observed along some sections of the Oman crust where it was attributed to extreme degrees of fractional crystallization made possible by the specific context of the leading edge of a magma chamber (Lachize et al., 1996; Boudier et al., 2000; Adachi and Miyashita, 2003). This mechanism of differentiation cannot account alone for the early crystallizing opx present in the Bahla lower crust.

Considering the mineral major and minor element compositions, the global decrease in Cr in pyroxenes, Ni in olivine and An of plagioclase, and the increase of Ti in pyroxenes with the decrease in XMg (Fig. 10) indicate that fractional crystallization actually contributed to some extent to the evolution of the parent melts of all the cumulates of Bahla. The opx-bearing lithologies also have clinopyroxene with higher trace incompatible element concentrations, especially in REE (Fig. 11). However, (1) the incompatible minor and trace elements concentrations show a significant variability for a given XMg, *even in a single lithological group*, and (2) there is a general lack of consistency between the modal composition and the chemical indexes of differentiation (Fig. 12). These are not characteristics unique to Bahla (cf.

Abily, 2011) but they are particularly evident in the case of this massif. This suggests that fractional crystallization from a common parent melt cannot solely account for this chemical variability and does not explain the relationships between the various lithologies. Among others, many cumulate harzburgites, dunites, wehrlites and pyroxenites, that would be considered as primitive on mineralogical grounds, may present quite evolved mineral compositions (Fig. 10), which is counter intuitive in the frame of cumulates issued from a single parent melt. The opx-troctolites constitute, apart from a few exceptions, a quite homogeneous group at the most evolved end of the chemical trends, especially in major elements. From a chemical perspective, the opx-troctolites share some characteristics with the most evolved samples from the gabbronorite group but the abundance of early crystallizing olivine and plagioclase is puzzling.

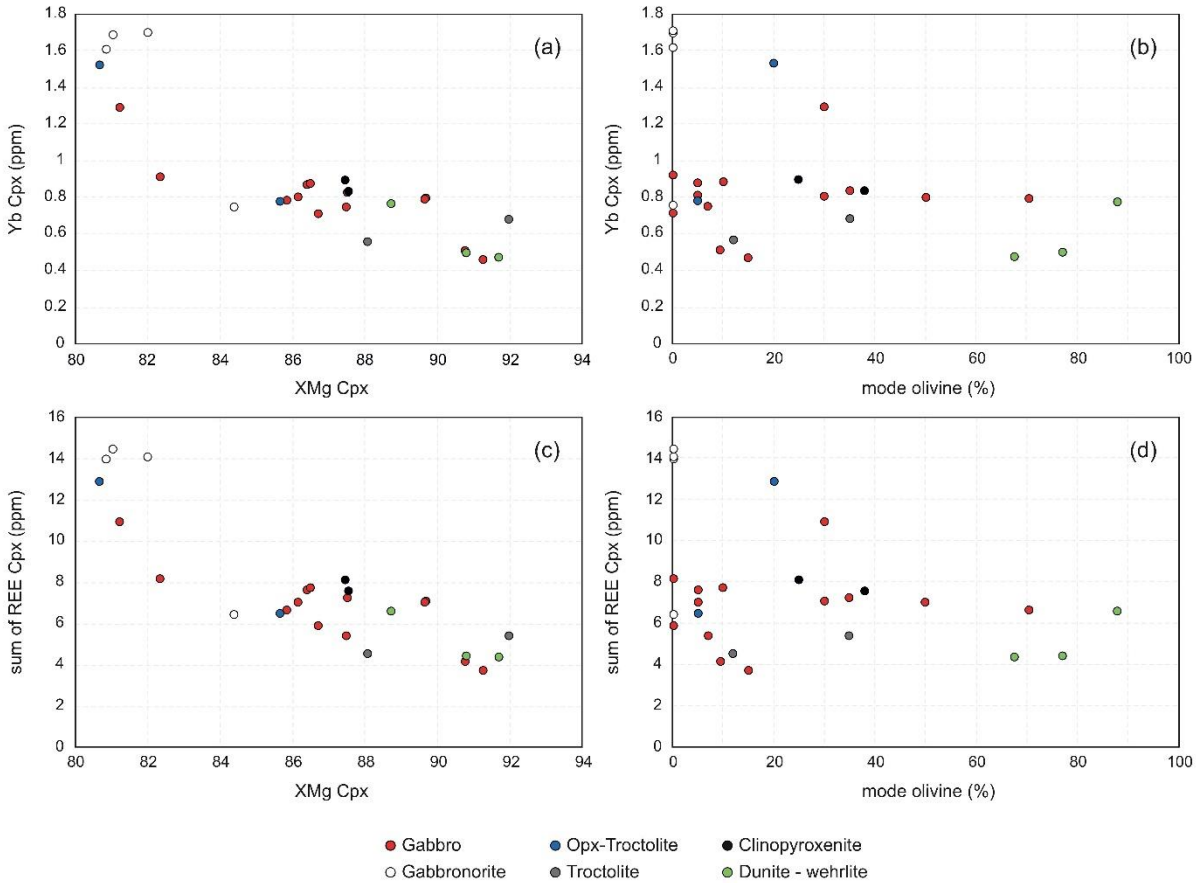

Fig. 12. Yb and sum of REE in clinopyroxene reported as a function of XMg of clinopyroxene and of modal content of olivine.

It is tempting to group the seven lithological groups identified in the Bahla lower crust in two main series as we did for the mantle dykes (Python and Ceuleneer, 2003): one whose mineralogical assemblage and crystallization order fit with an olivine tholeiite, MORB-like, parent melt (i.e. the troctolites, the olivine gabbros and the evolved gabbronorites) and another one including all the lithologies that do not fit a tholeiitic parent melt, i.e. most ultramafic cumulates (cumulate harzburgites, wehrlites, pyroxenites) and the opx-troctolites. The problem is that, contrasting with the mantle dykes, the geochemical composition of Bahla cumulates do not define two contrasted trends that would be diagnostic of a melt produced from a MORB mantle source on one hand and from a highly depleted mantle source on the other hand. As a matter of fact, the geochemical compositions of our different lithologies largely overlap.

In detail, the total REE content of cpx in the second group, except the opx-troctolites, is in the lower part of the variation field of Bahla cumulates and, more generally, of the lower crustal cumulates of Oman. However, the different lithologies do not contrast markedly in the shape of their REE patterns, showing that they did not crystallize from melts that are issued from a dramatically different degree of partial melting of the mantle source. The ultramafic cumulates and opx-rich gabbro display a less pronounced negative Sr anomaly in their extended trace element patterns than the troctolites and olivine gabbros. It results from a similar to lower Nd content but also from a slightly higher Sr content (higher than 9 µg/g while below 8 µg/g for other lithologies). This could be an effect of Sr depletion from the melt related to early plagioclase crystallization in troctolites and olivine gabbros, but it is not reflected in the Eu anomalies, which are mostly absent in all lithologies. The other difference between the two series is higher Ni (> 200 µg/g) and Cr (> 4000 µg/g) contents in clinopyroxene from the ultramafic lithologies (dunites and pyroxenites).

Magma mingling/mixing between the two contrasting melts identified in the mantle dykes of Oman is among the possible processes of the petrological characteristics of the Bahla lower crust. Although it is far from being a unique explanation, it is a simple way to account for the departure from simple fractional crystallization trends and for the poor contrast of the geochemical signatures between the various lithologies. Another avenue of explanations is variable input of water from a subducted slab (Koepke et al., this issue).

At the massif scale, we do not observe a geographical partitioning of the different types of cumulates. Several lithologies coexist in adjacent layers showing that the mixing was sufficiently incomplete to preserve the contrast in modal composition down to the outcrop scale.

We propose that deformation related to the first stages of activity of the high temperature ductile faults might have induced the mingling and the compaction of the crystal mush. In this model, interstitial melts, more or less hydrous and in variable stage of differenciation, were expelled and partially mixed at a local scale. Rapid crystallization, possibly triggered by the circulation of hydrothermal or subduction-derived fluids along the faults, made possible the preservation of contrasted lithological facies and of a certain heterogeneity in the chemical compositions. Mixing of the melts from both series identified in the mantle dyke population may have contributed to attenuate the contrast in incompatible elements signatures between the two series. The peculiar opx-troctolite lithology could be issued from an evolved tholeiitic melt relatively enriched in Ti and total REE due to fractional crystallization, whose cotectic trajectories has been modified by late mixing with a silica and Mg richer andesitic melt. Higher water concentration, whatever its origin, may have also contributed to its genesis as attested the presence of igneous amphibole in this facies. Such special conditions and petrological processes might also account for the compositional gap in the Fo of olivine which remains mysterious.

The origin of the MORB parent melt is not a real issue in the oceanic spreading setting that led to the accretion of the ophiolite. They can be formed at both mid-ocean ridges and in back-arc basins (although the absence of a mature arc along the northern margin of Arabia makes this late interpretation difficult). The genesis of the primitive andesite parent melt is also an open question in the specific context of the Oman ophiolite. Most authors working in Oman attribute such melts to mantle melting in the context of subduction. A challenging hypothesis is to consider that the genesis of opx-rich cumulates and of their parent melts is a natural consequence of the interaction between the mantle and lower crustal rocks and deep-seated hydrothermal fluids in a spreading setting, made possibly by the cyclic nature of the accretion process and triggered by faulting (Benoit et al., 1999; Clénet et al., 2010; Abily et al., 2011; Koepke et al., 2014; Rospabé et al., 2019). The formation of primitive gabbronorite dykes in response to the hydrated re-melting of the mantle along detachment faults is not unique to the Oman ophiolite (cf. Liu et al., 2014). Opx-rich, or at least bearing, primitive cumulates have been sampled along present-day mid-ocean ridges (both low and fast spreading) where the influence of subduction can be excluded in both slow-spreading (Nonnotte et al., 2005) and fast-spreading contexts Gillis et al., 2014). In spite of their discrete occurrences, and different textures in the case of fast spreading ridges, these lithologies exist in “open” mid-ocean settings and nurture discussions about their use to constrain the tectonic setting of ophiolites.

Although the present study is far from bringing definitive arguments allowing us to decipher between these hypotheses, it contributes to illustrate one among many tectonic contexts leading to the interaction and crystallization of two magmatic series that contributed to the building and igneous evolution of the Oman ophiolite.

5.6. Possible tectonic context of accretion of the Bahla massif.

The intense deformation experienced by the layered cumulates of Bahla occurred in very high temperature conditions and records a normal fault movement. This kinematic calls for extensional tectonics and is more consistent with a syn-accretion event rather than with the compressive context that prevailed during the early intra-oceanic thrusting or nascent subduction of the ophiolite that preluded the obduction.

It is tempting to see in the Bahla massif an analogue of the oceanic core complexes mapped along present-day slow-spreading ridges (e.g. Blackman et al., 1998) and in arc-related basins (e.g. Harigane et al., 2011. However, the great variability of present-day core complexes in terms of size, deformation structures, lithologies and, mostly, the fact that the pristine morphology and seafloor rock exposure of the Bahla massif at the time of accretion is not preserved due to erosion make a detailed comparison difficult. It remains that some characteristics of the Bahla massif may support this working hypothesis. Among others, the lithological diversity of the Bahla crustal section is strikingly reminiscent of the rocks sampled in this context of intense normal faulting, including ultramafic, troctolitic, gabbroic and gabbronoritic cumulates, trondhjemites and post-deformation gabbro dykes (e.g. Cannat and Casey; 1995; Cannat et al., 1997; Dick et al., 2008 and 2010).

The intersection between a spreading ridge and a transform fault is a setting where oceanic core complexes commonly develop. Among such so-called “intersection massifs”, those to the south of the Kane Fracture zone (Dick et al., 2008 and 2010) were particularly well surveyed. There, the concept of “plutonic growth faults” was introduced to account for addition of magma directly to the lower crust with minor counterparts in the erupted lavas. This context is favourable to the deformation and rotation of the lower crustal cumulates at an early stage of crystallization. This tectonic imprint pre-dates the last magmatic pulses as attested by the frequent occurrence of cross-cutting dykes (gabbro, diorite and diabase) in the dredged samples (Dick et al., 2010) and by the local imprint of very high temperature ductile deformation recording normal faults kinematic as observed in the cores sampled during the ODP Leg 153, Holes 921-923 (Cannat et al., 1997; Fletcher et al., 1997).

The detachment faults along present-day core complexes have variable extents along strike, ranging from a minimum of about 15 km to several tens of kilometres. They are interrupted longitudinally by faults sub-perpendicular to the spreading axis. In the context of intersection massifs, high and low temperature mylonites develop along one edge in response to the strike-slip tectonics induced by the transform fault (Dick et al., 2010). Brittle faults (breccias and cataclasites) are the rule at the other end of the detachment fault. This is remarkably close to the situation observed at Bahla. According to recent scenarios of formation and evolution of oceanic core complexes (e.g. Brun et al., 2018), the sense of rotation of the gabbro layering approaching the northern fault is consistent with a spreading ridge located to the ENE of Bahla. In this case, the Bahla massif would have formed along the WSW flank of the spreading center. This is in agreement with the fact that a paleo-ridge segment, witness of the last spreading activity recorded by the Oman ophiolite, has been frozen about 30 km to the NE of the Bahla massif, in a more internal part of the ophiolite (Ceuleneer, 1991; Ceuleneer et al., 1996; Nicolas et al., 2000; Python and Ceuleneer 2003). To invoke ridge jumps is another possibility. In this case, the accretion could have stopped along the internal paleo-ridge segments before the accretion of the Bahla massif, in reaction to the complex changes in stress field that likely preluded the inversion from divergence to convergence.

A major difference with the present-day core complexes is the non-cylindrical geometry at Bahla where the strike slip mylonitic fault is oriented at about 45° from the main detachment and has a significant normal fault component. This fault pattern evokes a context of a pull apart basin developing in response to north-westward ridge propagation and oblique extension. Ridge propagation has been invoked to account for complex structuration in the Oman ophiolite, in particular the cross-cutting relationships in the gabbroic section and in the sheeted dyke complex (e.g. Reuber, 1988; MacLeod and Rothery, 1992). It has been related to the reorganization of the plate motion that characterizes upper Cretaceous times (e.g. Stampfli and Borel, 2002) and that eventually resulted in the major episode of ophiolite emplacement on the Arabian margin (Ceuleneer, 1986; Agard et al., 2007). The accretion of the Oman ophiolite occurred during the regional inversion of extension to convergence, the main evidence being provided by the overlap between the crystallization ages of the evolved crustal lithologies dated so far and the ages of amphibolites from the metamorphic sole. The stress field in which the future ophiolite accreted was likely already partly impacted by this major reorganization which favoured the opening of pull-apart basins, ridge propagation and/or ridge jumps.

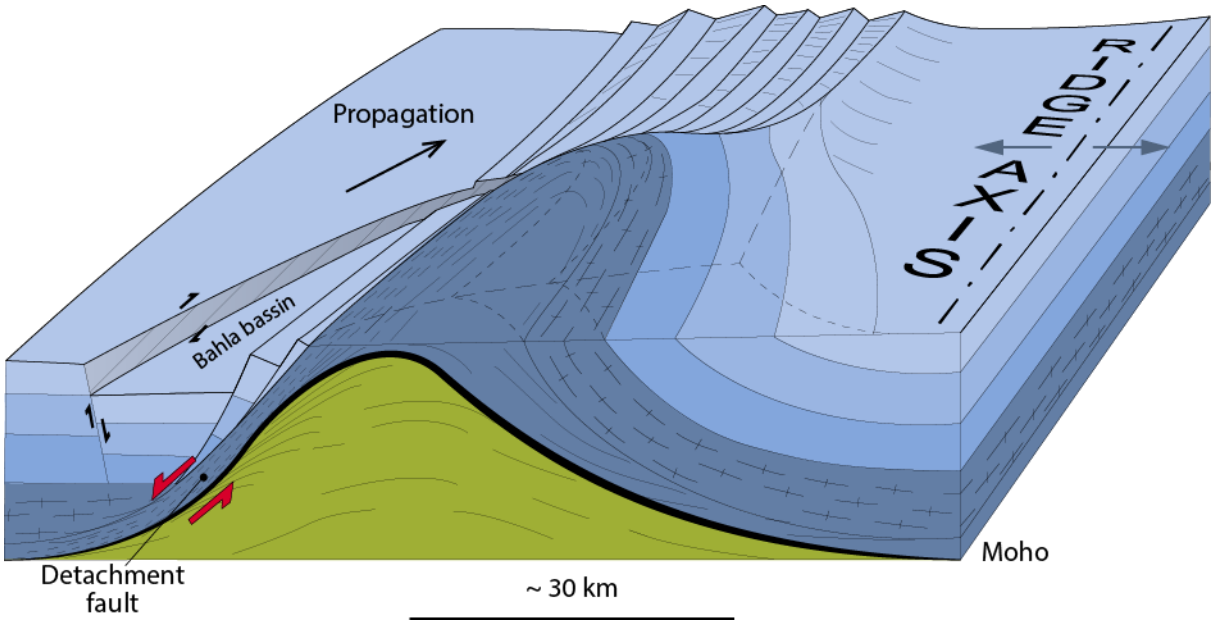

Fig. 13. A simplistic sketch illustrating a possible tectonic context for the formation of the Bahla massif (propagation is to the NW). Modified from Brun et al. (2018).

Accordingly, we tentatively interpret the Bahla massif as a witness of the opening of small pull-apart oceanic basins in a context of northward ridge propagation along the Oman continental margin (Fig. 13). The age of the plagiogranite (95.2 Ma) provides a minimum estimate of the age of accretion. It formed during the late stages of activity of the Bahla syn-accretion faults and early stages of intra-oceanic thrusting or nascent subduction. While the deformation along the main normal fault stopped early, permitting the preservation of high temperature structures with very minor overprint of low temperature deformation and alteration, the mylonitic strike slip fault was likely active a bit longer, up to the emplacement of the plagiogranite plug whose source was contaminated by melts or fluids from the nascent metamorphic sole.

In the present-day setting, the life time of plutonic growth faults and of related igneous activity (including the last dyke injection events in off-axis position) is rather well constrained by magnetic data and rock sampling in present-day setting; it is of the order of 1 to 2 million years (Dick et al., 2008). Accordingly, we can guess that igneous accretion started at Bahla 96 to 97 million years ago. As plutonic growth faults are common features at slow spreading centres, the opening of the Semail basin may have started in slow spreading conditions before evolving, for a short period of time, into fast spreading before the death of the system preluding the compressive movements. Alternately, plutonic growth faults might exist in fast spreading

settings where they are hidden below lava flow due to higher extrusive rates (e.g. Sauter et al., 2021).

6. Conclusion

Early faulting and its consequences are not included in oceanic accretion models inspired by studies in Oman. The local impact of syn-magmatic faults was initially revealed by field and petrological studies in the Maqsad area (Abily et al., 2011; Rospabé et al., 2019). Evidence from the Bahla massif indicate that former plutonic growth faults can condition the general structure and influence the petrological evolution of entire massifs, i.e. at a much larger scale.

The data presented in this paper led us to reconsider some common views about the tectonic setting of the Oman ophiolite, and to speculate about its possible evolution. The Oman ophiolite is a complex heterogeneous geological object. Clearly, the paradigm of viewing the Oman ophiolite *as a whole* as the archetype for fast-spreading oceanic crust accretion (whether mid-ocean ridge or subduction related) should be nuanced.

Acknowledgements

We greatly appreciated the comments from reviewers Thomas Belgrano and Tomoaki Morishita and from the associate editor Juergen Koepke that contributed to improve the manuscript. We are thankful to Mohamed Al Araimi, Ali Al Rajhi, Mohamed Al Batashi, Said Al Musharrafi and Ibrahim Al Sawafi from the Public Authority of Mining of Oman for their support and for making fieldwork in Oman possible. We thank Philippe de Parseval and Sophie Gouy for their help in the acquisition of the electron microprobe analyses, to Fabienne de Parseval who made the numerous thin sections necessary for this study and to AnneMarie Cousin for her help in designing the figures. Financial support was provided by CNRS-INSU.

References.

Abily B. Caractéristiques pétrographique, géochimique et structural de la section crustale profonde de l'ophiolite d'Oman : implications pour la genèse des magmas et le fonctionnement des chambres magmatiques à l'aplomb d'un centre d'expansion océanique. Thèse de l'Université Paul Sabatier, Toulouse III, 685 pp., 2011.

Abily B. and Ceuleneer G. The dunitic mantle-crust transition zone in the Oman ophiolite: Residue of melt-rock interaction, cumulates from high-MgO melts, or both? Geology, 41, 67-70, 2013.

959 Abily B., Ceuleneer G. and Launeau P. Syn-magmatic normal faulting in the lower oceanic crust: evidence
960 from the Oman ophiolite. Geology, 39, 391-394, 2011.

961 Adachi Y. and Miyashita S. Geology and petrology of the plutonic complexes in the wadi Fizh area: multiple
962 magmatic events and segment structure in the northern Oman ophiolite. Geochem. Geophys. Geosyst., 4(9), 8619,
963 doi :10.1029/2001 GC000272, 2003.

964 Agard P., Jolivet L., Vrielynck B., Burov E. and Monié P. Plate acceleration : the obduction trigger ? Earth
965 Planet. Sci. Lett., 258, 428-441, 2007.

966 Agard P., Prigent C., Soret M., Dubacq B., Guillot S. and Deldicque D. Stabilization: mechanisms controlling
967 subduction development and viscous coupling. Earth-Science Reviews, 208, 103259, 2020.

968 Alabaster T., Pearce J.A., Malpas J. The volcanic stratigraphy and Petrogenesis of the Oman Ophiolite
969 complex. Contrib. Mineral. Petrol., 81, 168-183, 1982.

970 Andronicos C.L., Phipps Morgan J., Chang J.M. and Wolf D.E. Melt-filled hybrid fractures in the oceanic
971 mantle : melt enhanced deformation during along-axis flow beneath a propagating spreading ridge axis. Earth
972 Planet. Sci. Lett., 273, 270-278, 2008.

973 Bach, W., and Klein, F. The petrology of seafloor rodingites: Insights from geochemical reaction path
974 modelling. Lithos, v. 112, no. 1-2, p. 103-117, 2009.

975 Béchennec, F., Roger, J., Le Métour, J., and Wyns, R.. Explanatory notes to the Geological Map of Seeb,
976 Sheet NF40-03, Scale: 1:250,000. Directorate General of Minerals, Oman Ministry of Petroleum and Minerals,
977 1992.

978 Belgrano T.M. and Diamond L. Subduction-zone contribution to axial volcanism in the Oman-U.A.E.
979 ophiolite. Lithosphere, 11, 399-411, 2019.

980 Belgrano T.M., Diamond L.W., Vogt Y., Biedermann A. R., Gilgen S.A. and Al-Tobi K. A revised map of
981 volcanic units in the Oman ophiolite: insights into the architecture of an oceanic proto-arc volcanic sequence. Solid
982 Earth, 10, 1181-1217, 2019.

983 Ben Ismail W. and Mainprice D. An olivine fabric database: an overview of upper mantle fabrics and seismic
984 anisotropy. Tectonophysics, 296, 145-157, 1998.

985 Benoit M., Ceuleneer G. and Polvé M. The remelting of hydrothermally altered peridotite at mid-ocean ridges
986 by intruding mantle diapirs. Nature, 402, 514-518, 1999.

987 Blackman, D. K., Cann, J. R., Janssen, B., Smith, D. K. Origin of extensional core complexes: Evidence from
988 the Mid-Atlantic Ridge at Atlantis Fracture Zone. Journal of Geophysical Research-Solid Earth, v. 103, p. 21315-
989 21333, 1998.

990 Boudier, F., Ceuleneer, G., and Nicolas, A. Shear Zones, Thrusts and Related Magmatism in the Oman
991 Ophiolite: Initiation of Thrusting on an Oceanic Ridge. Tectonophysics, v. 151, no. 1-4, p. 275-296, 1988.

992 Boudier F. and Nicolas A. Nature of the Moho transition zone in the Oman ophiolite. J. Petrol., 36, 777-796,
993 1995.

994 Boudier F., Godard M. and Armbruster C. Significance of gabbronorite occurrence in the crustal section of
995 the Semail ophiolite. Mar. Geophys. Res., 21, 307-326, 2000.

996 Boudier, F., and Nicolas, A. Comment on "Dating the geologic history of Oman's Semail ophiolite: insights
997 from U-Pb geochronology" by C. J., Warren, R. R., Parrish, D. J., Waters and M. P., Searle. Contributions to
998 Mineralogy and Petrology, v. 154, no. 1, p. 111-113, 2007.

Bunge, H.J., 1982. Texture analysis in materials science: mathematical methods. Elsevier.

Breton J.-P., Béchennec F., Le Métour J., Moen-Maurel L. and Razin P. Eoalpine (Cretaceous) evolution of the Oman tethyan continental margin: insights from a structural field study in Jabal Akhdar (Oman mountains). GeoArabia, 9, 231-248, 2004.

Brey G. P. and Köhler T. Geothermobarometry in four-phase lherzolites II. New thermobarometers, and practical assessment of existing thermobarometers. Journal of petrology. v. 31 i. 6, p. 1353, 1378, 1990.

Browning P. Cryptic variation within the cumulate sequence of the Oman ophiolite: magma chamber depth and petrological implication. In: Malpas et al (Eds), Ophiolites - Oceanic crustal analogue. Geol. Surv. Dep., Cyprus, Nicosia, 71-82, 1990.

Brun J.-P., Sokoutis D., Tirel C., Gueydan F., Van Den Driessche J. and Beslier M.-O. Crustal versus mantle core complexes. Tectonophysics, 746, 22-45, 2018.

Cannat M. and Casey J. An ultramafic lift at the Mid-Atlantic Ridge: successive stages of magmatism in serpentinized peridotites from the 15°N region. In: Vissers R.L.M. and Nicolas A. (Eds), Mantle and lower crust exposed in oceanic ridges and ophiolites, Kluwer, 5-34, 1995.

Cannat M., Ceuleneer G. and Fletcher J. Localization of ductile strain and the magmatic evolution of gabbroic rocks drilled at the Mid-Atlantic Ridge. Ocean Drilling Progam, Scientific Results, volume 153, 77-98, 1997.

Ceuleneer G. Structure des ophiolites d'Oman : flux mantellaire sous un centre d'expansion océanique et charriage à la dorsale. Thèse de l'Université de Nantes, 349 pp., 1986.

Ceuleneer G. Evidence for a paleo-spreading center in the Oman ophiolite: mantle structures in the Maqsad area. In: T.J. Peters, Editor, "Ophiolite genesis and evolution of oceanic lithosphere", Kluwer Academic Press, 149-175, 1991.

Ceuleneer G., Monnereau M. and Amri I. Thermal structure of a fossil mantle diapir inferred from the distribution of mafic cumulates. Nature, 379, 149-153, 1996.

Ceuleneer G., Nicolas A. and Boudier F. Mantle flow patterns at an oceanic spreading centre: the Oman peridotites record. Tectonophysics, 151, 1-26, 1988.

Clénet H., Ceuleneer G., Pinet P., Abily B., Daydou Y., Harris E., Amri I. and Dantas C. Thick sections of layered ultramafic cumulates in the Oman ophiolite revealed by an airborne hyperspectral survey: petrogenesis and relationship to mantle diapirism. Lithos, 114, 265-281, doi:10.1016/j.lithos.2009.09.002, 2010.

Coleman, R. G. Tectonic Setting for Ophiolite Obduction in Oman. Journal of Geophysical Research, 86, 2497-2508, 1981.

De Graaf S.J., Goodenough K.M., Klaver M., Lissenberg C.J., Jansen M.N., Millar I and Davies G.R. Evidence for a moist to wet source transition throughout the Oman-UAE ophiolite, and implications for the geodynamic history. Geochem., Geophys., Geosyst., 20, 651-672, 2019.

Díaz-Azpiroz M., Lloyd G.E. and Fernández C. Deformation mechanisms of plagioclase and seismic anisotropy of the Acebuches metabasites (SW Iberian massif). Geological Society, London, Special Publications 360 (1), 79-95, 2011.

Dick, H. J. B., Tivey, M. A., and Tucholke, B. E.. Plutonic foundation of a slow-spreading ridge segment: Oceanic core complex at Kane Megamullion, 23°30'N, 45°20'W. Geochemistry Geophysics Geosystems, v. 9, 2008.

Dick, H. J. B., Lissenberg J. and Warren J.M. Mantle melting, melt transport, and delivery beneath a slow-spreading ridge: the paleo-MAR from 23°15'N to 23°45'N. J. Petrol., 51, 425-467, 2010.

1040 Einaudi F., Godard M., Pezard P., Cochemé J.-J., Coulon C., Brewer T. and Harvey P. Magmatic cycles and
1041 formation of the upper oceanic crust at spreading centers : geochemical study of a continuous extrusive section in
1042 the Oman ophiolite. Geochem. Geophys. Geosyst., 4(6), 8608, doi :10.1029/2002 GC000362, 2003.

1043 Ernewein, M., Pflumio, C. et Whitechurch, H. The death of an acretion zone as evidenced by the magmatic
1044 history of the Sumail ophiolite (Oman), Tectonophysics, 151, 247-274, 1988.

1045 Escartin J., Smith D.K., Cann J., Schouten H., Langmuir C.H. and Escrig S. Central role of detachment faults
1046 in accretion of slow-spreading oceanic lithosphere. Nature, 455, 790-794, 2008.

1047 Fletcher, J., Ceuleneer G. and Cannat M. Microfabrics and patterns of dynamic recrystallization in gabbroic
1048 rocks from the MARK area, Mid-Atlantic Ridge. In : Karson J.A., Cannat M., Miller D.J. and Elthon D., Eds.,
1049 Proc. Ocean Drilling Progam, Scientific Results, 153, College Station, Texas, U.S.A., 143-153, 1997.

1050 Gillis K.M., Snow J.E., Klaus A., Abe N., de Brito Adriao A., Akizawa N., Ceuleneer G., Cheadle M., Faak
1051 K., Falloon T., Friedman S., Godard M., Guerin G., Harigane Y., Horst A., Hoshide T., Ildefonse B., Jean M.M.,
1052 John B.E., Koepke J.H., Machi S., Maeda J., Marks N.E., McCaig A.M., Meyer R., Morris A., Nozaka T., Python
1053 M., Saha A., Wintsch R.P. Primitive layered gabbros from fast-spreading lower oceanic crust. Nature, 505, 204-
1054 207, 2014.

1055 Glennie K.W., Boeuf M.G.A., Hughes-Clark M.W., Moody-Stuart M., Pilaar W.F.H. and Reinhardt B.M.
1056 Late cretaceous nappes in Oman mountains and their geologic evolution. Amer. Assoc. Petrol. Geol. Bull., 57, 5-
1057 27, 1973.

1058 Godard M., Bosch D. and Einaudi F. A MORB source for low-Ti magmatism in the Semail ophiolite. Chem.
1059 Geol., 234, 58-78, 2006.

1060 Goffé, B., Michard, A., Kienast, J.R. et LeMer, O. A case of obduction-related high-pressure, low-
1061 temperature metamorphism in upper crustal nappes, Arabian continental margin, Oman: P-T path and kinematic
1062 interpretation, Tectonophysics, 151, 363-386, 1988.

1063 Goodenough K.M., Thomas R.J., Styles M.T., Schofield D.I. and MacLeod C.J. Records of ocean growth
1064 and destruction in the Oman-UAE ophiolite. Elements, 10, 109-114, 2014.

1065 Granot, R., Dyment, J., & Gallet, Y. Geomagnetic field variability during the Cretaceous Normal Superchron.
1066 Nature Geoscience, 5(3), 220-223, 2012.

1067 Gray D.R., Hand M., Mawby J., Armstrong R.A., Miller J.McL. and Gregory R.T. Sm-Nd and zircon U-Pb
1068 ages from garnet-bearing ecolgites, NE Oman: constraints on high-P metamorphism. Earth Planet. Sci. Lett., 222,
1069 407-422, 2004.

1070 Gray D.R., Gregory R.T. and Miller J.McL. Comment on “Structural evolution, metamorphism and
1071 restoration of the Arabian continental margin, Saih Hatat region, Oman mountains” by M.P. Searle et al. J. Struct.
1072 Geol., 27, 371-374, 2005.

1073 Griffin, W.L., 2008. Laser ablation ICP-MS in the Earth Sciences : current practices and outstanding issues.
1074 Mineral. Assoc. Can. 40, 308–311.

1075 Haase K.M., Freund S., Beier C., Koepke J., Erdmann M. and Hauff F. Constraints on the magmatic evolution
1076 of the oceanic crust from plagiogranite intrusions in the Oman ophiolite. Contrib. Mineral. Petrol., 171:46, DOI
1077 10.1007/s00410-016-1261-9, 2016.

1078 Harigane Y., Michibayashi K. and Ohara Y. Deformation and hydrothermal metamorphism of gabbroic rocks
1079 within the Godzilla megamullion, Parece Vela Basin, Philippine Sea. Lithos, 124, 185-199, 2011.

1080 Hopson C.A., Coleman R.G., Gregory R.T., Pallister J.S. and Bailley E.H. Geologic section through the
1081 Samail Ophiolite and associated rocks along the Muscat-Ibra transect, southeastern Oman Mountains. J. Geophys.
1082 Res., 86, 2527-2544, 1981.

1083 Ildefonse, B., Blackman, D. K., John, B. E., Ohara, Y., Miller, D. J., MacLeod, C. J., and Integrated Ocean
1084 Drilling Program Expeditions 304/305 Science Party. Oceanic core complexes and crustal accretion at slow-
1085 spreading ridges. Geology, 35, 623-626, 2007.

1086 Irvine, T. N. Terminology for Layered Intrusions. Journal of Petrology, v. 23, no. 2, p. 127-162, 1982.

1087 Ishikawa T., Fujisawa S., Nagaishi K. and Masuda T. Trace element characteristics of the fluid liberated from
1088 amphibolite facies slab : inference from the metamorphic sole beneath the Oman ophiolite and implication for
1089 boninite genesis. Earth Planet. Sci. Lett., 240, 355-377, 2005.

1090 Jousselin D. and Nicolas A. Oceanic ridge off-axis deep structure in the Mansah region (Sumail massif, Oman
1091 ophiolite). Mar. Geophys. Res., 21, 243-257, 2000.

1092 Juteau, T., Ernewein, M., Reuber, I., Whitechurch, H., and Dahl, R. Duality of Magmatism in the Plutonic
1093 Sequence of the Sumail Nappe, Oman. Tectonophysics, v. 151, no. 1-4, p. 107-135, 1988.

1094 Karato S. Deformation of earth materials: an introduction to the rheology of solid earth. Cambridge Univ
1095 Press, 463 pp., 2008.

1096 Kelemen P.B., Koga K. and Shimizu N. Geochemistry of gabbro sills in the crust/mantle transition zone of
1097 the Oman ophiolite: implications for the origin of the oceanic lower crust. Earth Planet. Sci. Lett., 146, 475-488,
1098 1997.

1099 Koepke J., Schoenborn S., Oelze M. Wittmann H., Feig S.T., Hellebrand E., Boudier F. and Schoenberg R.
1100 Petrogenesis of crustal wehrlites in the Oman ophiolite: experiments and natural rocks. Geochem. Geophys.
1101 Geosyst., 10, Q10002, 2009.

1102 Koepke J., Berndt J., Horn I., Fahle J. and Wolff P.E. Partial melting of oceanic gabbro triggered by migrating
1103 water-rich fluids: a prime example from the Oman ophiolite. In: Rollinson H.R., Searle M.P., Abbasi I.A., Al-
1104 Lazki A. and Al Kindi M.H. Eds. Tectonic evolution of the Oman Mountains. Geol. Soc. London, Spec. Pub., 392,
1105 195-212, 2014.

1106 Korenaga, J. and Kelemen, P. B. Origin of gabbro sills in the Moho transition zone of the Oman ophiolite:
1107 Implications for magma transport in the oceanic lower crust. Journal of Geophysical Research: Solid Earth,
1108 102(B12), 27729-27749, 1997.

1109 Kruse R. Stünitz H. and Kunze K. Dynamic recrystallization processes in plagioclase porphyroclasts, J.
1110 Struct. Geol., 23, 1781-1802, 2001.

1111 Lachize M., Lorand J.-P. and Juteau T. Calc-alkaline differentiation trend in the plutonic sequence of the
1112 Wadi Haymiliyah section, Haylayn massif, Semail ophiolite, Oman. Lithos, 38, 207-232, 1996.

1113 Liu C.-Z., Zhang C., Yang L.-Y., Zhang L.-L., Ji W.-Q. and Wu F.Y. Formation of gabbronorites in the
1114 Purang ophiolite (SW Tibet) through melting of hydrothermally altered mantle along a detachment fault. Lithos,
1115 205, 127-141, 2014.

1116 MacLeod, C.J. et Rothery, D.A. Ridge axial segmentation in the Oman ophiolite: evidence from along-strile
1117 variations in the sheeted dyke complex, In: L.M. Parson, B.J. Murton and P. Browning, Eds, in Geol. Soc. Spec.
1118 Pub., 60, 39-63, 1992.

1119 MacLeod C.J., Escartin J., Banereji D., Banks G.J., Gleeson M., Irving D.H.B., Lilly R.M., McCaig A.M.,
1120 Niu Y., Allerton S. and Smith D.K. Direct geological evidence for oceanic detachment faulting: the Mid-Atlantic
1121 Ridge, 15°45'N. Geology, 30, 879-882, 2002.

McDonough, W. F., and Sun, S. S., (1995). The Composition of the Earth. Chemical Geology, v. 120, no. 3-4, p. 223-253.

MacLeod C.J., Lissnberg C.J., and Bibby L.E. “Moist MORB” axial magmatism in the Oman ophiolite: the evidence against a mid-ocean ridge origin. Geology, 41, 459-462, 2013.

MacLeod, C. J., and Rothery, D. A. Ridge axial segmentation in the Oman ophiolite: evidence from along-strike variations in the sheeted dyke complex. In “Ophiolites and their Modern Oceanic Analogues”, Parson, L. M., Murton, B. J., & Browning, P., (Eds), Geological Society Special Publication, v. 60, no. 1, p. 39-63, 1992.

Marshall D.B. and McLaren A.C. The direct observation and analysis of dislocations in experimentally deformed plagioclase feldspars. Journal of Materials Science, 12, pages 893–903, 1977.

Müller, T. A petrological and geochemical cross section of lower crust at the Wadi Gideah (Samail ophiolite): Implications for the crustal accretion at fast-spreading mid-ocean ridges. Doctoral dissertation, Université de Montpellier, 2015.

Nicolas A., Bouchez J.-L. Boudier F. and Mercier J.-C. Textures, structures and fabrics due to solid state flow in some european lherzolites. Tectonophysics, 12, 55-86, 1971.

Nicolas, A., Boudier, E., Ildefonse, B., and Ball, E. Accretion of Oman and United Arab Emirates ophiolite - Discussion of a new structural map. Marine Geophysical Researches, v. 21, no. 3-4, p. 147-179, 2000.

Nonnotte P., Ceuleneer G. and Benoit M. Genesis of andesitic-boninitic magmas at mid-ocean ridges by melting of hydrated peridotites : geochemical evidence from DSDP Site 334 gabbronorites. Earth Planet. Sci. Lett., 236, 632-653, 2005.

Olsen T.S. and Kohlstedt D.L. Analysis of dislocations in some naturally deformed plagioclase feldspars. Physics and chemistry of minerals, 11, 153-160, 1984.

Pallister J.S. and Hopson C.A. Samail ophiolite plutonic suite: field relations, phase variations, cryptic variation and layering, and a model of a spreading Ridge magma chamber, J. Geophys. Res., 86, 2593-2644, 1981.

Pallister J.S. and Knight R.J. Rare-Earth element geochemistry of the Samail ophiolite near Ibra, Oman. J. Geophys. Res., 86, 2673-2698, 1981.

Pearce, J. A., Alabaster, T., Shelton, A. W., and Searle, M. P. The Oman Ophiolite as a Cretaceous Arc-Basin Complex: Evidence and Implications. Philosophical Transactions of the Royal Society of London Series a - Mathematical Physical and Engineering Sciences, v. 300, no. 1454, p. 299-317, 1981.

Python M. and Ceuleneer G. Nature and distribution of dykes and related melt migration structures in the mantle section of the Oman ophiolite. Geochem. Geophys. Geosyst., 4(7), 8612, doi :10.1029/2002 GC000354, 2003.

Python M., Ishida Y., Ceuleneer G. and Arai S. Trace element heterogeneities in hydrothermal diopsides : evidence for Ti-HREE depletion and Sr-Eu-LREE enrichment during hydrothermal metamorphism of mantle harzburgites. J. Mineral. Petrol. Sci., 102(2), 143-149, 2007.

Python, M., Ceuleneer, G., and Arai, S. Chromian spinels in mafic-ultramafic mantle dykes: Evidence for a two-stage melt production during the evolution of the Oman ophiolite. Lithos, v. 106, no. 1-2, p. 137-154, 2008.

Python, M., Yoshikawa, M., Shibata, T. and Arai, S. Diopsidites and Rodingites: Serpentinisation and Ca-Metasomatism in the Oman Ophiolite Mantle. In “Dyke Swarms: Keys for Geodynamic Interpretation”, Srivastava, R. K., (Eds), Springer, chapter 23, p. 401-435, 2011.

Reuber I. Complexity of the crustal sequence in northern Oman ophiolite (Fizh and southern Aswad block): the effect of early slicing? Tectonophysics, 151, 137-165, 1988.

Ricou L.E. Le croissant ophiolitique peri-arabe, une ceinture de nappes mises en place au Crétacé supérieur. Rev. Géogr. Phys. Géol. Dyn. (2). XIII, 4, 327-350, 1971.

Rioux M., Bowring S., Kelemen P., Gordon S., Dudas F. and Miller R. Rapid crustal accretion and magma assimilation in the Oman-U.A.E. ophiolite : high precision U-Pb zircon geochronology of the gabbroic crust. J. Geophys. Res., 117, B07201, doi:10.1029/2012JB009273, 2012.

Rioux M., Bowring S., Kelemen P., Gordon S., Miller R. and Dudas F. Tectonic development of the Samail ophiolite: high precision U-Pb zircon geochronology and Sm-Nd isotopic constraints on crustal growth and emplacement. J. Geophys. Res., 118, B07201, doi:10.1002/jgrb.50139, 2013.

Rioux M., Garber J., Bauer A., Bowring S., Searle M., Kelemen P. and Hacker B. Synchronous formation of the metamorphic sole and igneous crust of the Semail ophiolite: new constraints on the tectonic evolution during ophiolite formation from high-precision U-Pb zircon geochronology. Earth Planet. Sci. Lett., 451, 185-195, 2016.

Rioux, M., Garber, J. M., Searle, M., Kelemen, P., Miyashita, S., Adachi, Y. and Bowring, S. High-precision U-Pb zircon dating of late magmatism in the Samail ophiolite: A record of subduction initiation. J. Geophys. Res., 126, e2020JB020758, 2021a.

Rioux, M., Benoit, M., Amri, I., Ceuleneer, G., Garber, J. M., Searle, M. and Leal, K. The origin of felsic intrusions within the mantle section of the Samail ophiolite: Geochemical evidence for three distinct mixing and fractionation trends. J. Geophys. Res., 126, e2020JB020760, 2021b.

Rospabé M., Ceuleneer G., Benoit M., Abily B. and Pinet P. Origin of the dunitic mantle-crust transition zone in the Oman ophiolite: The interplay between percolating magmas and high-temperature hydrous fluids. Geology, 45, 471-474, 2017.

Rospabé M., Benoit M., Ceuleneer G., Hodel F. and Kaczmarek M.-A. Extreme geochemical variability through the duntic transition zone of the Oman ophiolite: implications for melt/fluid-rock reactions at Moho level beneath oceanic spreading centers. Geochim. Cosmochim. Acta, 234, 1-23, 2018.

Rospabé M., Benoit M., Ceuleneer G., Kaczmarek M.-A. and Hodel F. Melt hybridization and metasomatism triggered by syn-magmatic faults within the Oman ophiolite: a clue to understand the genesis of the dunitic mantle-crust transition zone. Earth Planet. Sci. Let., 516, 108-121, 2019.

Ross J.V. and Nielsen K.C. High-temperature flow and wet polycrystalline enstatite. Tectonophysics, 44, 233-261, 1978.

Sauter D., Werner P., Ceuleneer G., Manatschal G., Rospabé M., Tugend J., Gillard M., Autin J. and Ulrich M. Sub-axial deformation of oceanic lower crust : insights from seismic reflection profiles in the Enderby basin and comparison with the Oman ophiolite. Earth and Planet. Sci. Lett., 554, 116698, 2021.

Searle M.P., Warren C.J., Waters D.J. and Parrish R.R. Structural evolution, metamorphism and restoration of the Arabian continental margin, Saih Hatat region, Oman mountains. J. Struct. Geol., 26, 451-473, 2004.

Smewing J.D. Mixing characteristics and compositional differences in mantle-derived melts beneath spreading axis: evidence from cyclically layered rocks in the ophiolite of North Oman, J. Geophys. Res., 86, 2645-2660, 1981.

Stampfli G.M. and Borel G.D. A plate tectonic model for the Paleozoic and Mesozoic constrained by dynamic plate boundaries and restored synthetic oceanic isochrons. Earth Planet. Sci. Lett., 196, 17-33, 2002.

Warren, C. J., Searle, M. P., Parrish, R. R., and Waters, D. J. Reply to comment by F. Boudier and A. Nicolas on "Dating the geologic history of Oman's Semail ophiolite: Insights from U-Pb geochronology" by C. J., Warren, R. R., Parrish, M. P., Searle and D. J., Waters. Contributions to Mineralogy and Petrology, v. 154, no. 1, p. 115-118, 2007.

1205 Warren C.J., Parrish R.R., Searle M.P. and Waters D.J. Dating the subduction of the arabian continental
1206 margin beneath the Semail ophiolite, Oman. Geology 31, 889-892, 2003.

1207 Wyns, R., Béchennec, F., Chevrel, S., Le Métour, J., and Roger, J. Explanatory notes to the Geological Map
1208 of Nazwa, Sheet NF40-07, Scale: 1:250,000. Directorate General of Minerals, Oman Ministry of Petroleum and
1209 Minerals, 1992.

1210 Yamasaki T., Maeda J. and Mizuta T. Geochemical evidence in clinopyroxenes from gabbroic sequence for
1211 two distinct magmatisms in the Oman ophiolite. Earth Planet. Sci. Lett., 251, 52-65, 2006.

1212 Yamato P., Agard P., Goffé B., De Andrade V., Vidal O. and Jolivet L. New, high-precision P-T estimates
1213 for Oman blueschists : implications for obduction, nappe stacking and exhumation processes. J. Metam. Geol., 25,
1214 657-682, 2007.

1215 Zihlmann B., Müller S., Coggon R.M., Koepke J., Garbe-Schönberg D. and Teagle D. Hydrothermal fault
1216 zones in the lower oceanic crust: an example from Wadi Gideah, Samail ophiolite, Oman. Lithos, 323, 103-124,
1217 2018.